A Tutorial on the Tracking, Telemetry, and Command (TT&C) for Space Missions

A Tutorial on the Tracking, Telemetry, and Command (TT&C) for Space Missions

Andrea Modenini, Barbara Ripani, *Student Member, IEEE*

***Abstract*—This paper presents a tutorial on the Tracking, Telemetry, and Command (TT&C) for spacecraft and satellite missions. In particular, it provides a thorough summary of the design of the TT&C, starting from elementary system aspects and going down to the details of the on-board TT&C subsystem design, its units, and the physical layer. The paper is then complemented with a description of emerging TT&C techniques and technologies, the standardization framework, and practical examples of actual spacecraft design of European space missions.**

The here-presented tutorial is thought for professionals (also in other telecommunication engineering fields) willing to face the challenges and state-of-the-art of the TT&C, and know more about this fundamental function that allows us to control and monitor our spacecraft on a daily basis.

***Index terms*—TT&C, PDT, Telecommand, Telemetry, Ranging, Transponder, Satellite**

I. Introduction

The TT&C is a critical function that ensures the flying system operates correctly. As depicted in Figure 1, the TT&C uses radio-frequency (RF) links between the space element and the ground. As the name suggests, it performs three fundamental tasks: *Command* (also known as *telecommand*, TC), *Telemetry* (TM), and *Tracking* (also denoted, with abuse of naming, simply as *ranging*, RNG). The TC function allows to send commands and thus control the spacecraft: the mission operation center (MOC) sends commands through an Earth-to-space data burst transmission. Since commands are simple data that trigger specific spacecraft actions, TC data rates are usually in the order of some kbps (or even bps). The TM is instead the monitoring function, which involves retrieving the spacecraft's recordings and status. This information is downloaded to the ground through a space-to-Earth link and then redirected to the MOC. Depending on the number and size of the spacecraft subsystems, TM data rates can range from kbps to Mbps. Finally, tracking is a function that aids the determination of the spacecraft's flight dynamics. Namely, an RNG signal is sent from the TT&C ground station to the spacecraft that, in turn, transposes it back to the ground (i.e., it does an *RNG turn-around*). In this way, the TT&C ground station can estimate the round-trip time and thus determine the distance from the spacecraft. Additionally, it can adopt the Doppler measure in the downlink to predict the spacecraft's radial velocity w.r.t. the ground station. Theoretically, the described TT&C links cover all directions for guaranteeing the mission data flow. However, spacecraft often carry a payload (e.g., scientific instruments) that produces high volumes of information. Thus, the TM link could be inadequate for downloading such an amount of data. Hence, the TT&C is often complemented with a dedicated payload data transmission (PDT) link, from the spacecraft to a dedicated payload ground station that redirects the received stream to the payload data center.

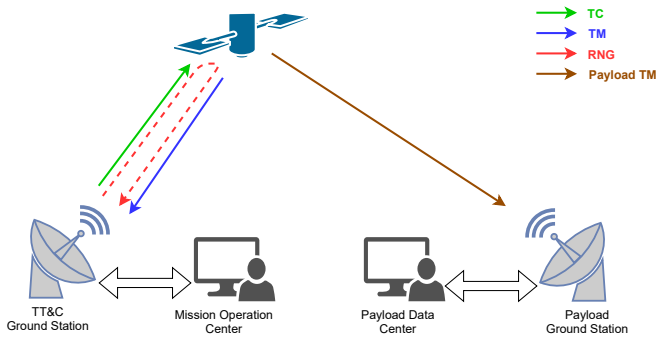

Figure 1. Sketch of the TT&C system: the ground segment can operate and monitor the spacecraft by means of the TC and TM links. The payload data can be instead retrieved by means of a dedicated payload TM link (if the TM link is not sufficient for performing such a function). The RNG is instead performed using a dedicated signal that is transposed back to the ground.

The TT&C has a crucial role in the success of any space mission. However, those attempting to review the existing literature can quickly realize that the topic is a "niche field": only a few companies have TT&C expertise, and public and academic material is scarce. Furthermore, the papers in this field tend to be highly technical and intended for those already knowledgeable in the subject.

Hence, this paper aims to provide a TT&C tutorial that offers an overview of the general concepts and the current state-of-the-art. The authors intentionally wrote Sections II and III to be accessible to any professional or student in the telecommunication field, facilitating their understanding of the TT&C basics. The following sections go deeper into the subject, providing mathematical formulas, tables, trade-off discussions, and extensive references, easing the transition to reading more advanced papers. The tutorial will include several examples, in support of the explanation, with particular reference to European technologies, standards, and European Space Agency (ESA) missions. Nevertheless, the here-

Andrea Modenini is with the European Space Agency at European Space Research and Technology Centre (ESA/ESTEC), 2201AZ Noordwijk, The Netherlands (email: andrea.modenini@esa.int).

Barbara Ripani is with Politecnico di Torino, Department of Electronics and Telecommunications (DET), I-10129 Torino, Italy (email: barbara.ripani@polito.it).

The view expressed herein can in no way be taken to reflect the official opinion of the European Space Agency.

This article has been accepted for publication in IEEE Communications Surveys & Tutorials. This is the author's version which has not been fully edited and content may change prior to final publication. Citation information: DOI 10.1109/COMST.2023.3287431

provided content can apply to non-European space missions of major space agencies such as NASA, JAXA, and CNSA since the standards and engineering described here are agreed upon at inter space-agency level.

On the other hand, it should be noted that this paper does not cover the basics of space engineering, such as satellite orbits, space qualification, technology readiness, and other related aspects, despite their relevance to TT&C engineering. According to the authors, these topics are well covered by the existing literature and are beyond the objective of this paper. Whenever these topics are mentioned, appropriate references will be provided. For readers seeking an overview of space mission engineering, readings such as [1] and [2] serve as good starting points.

The remainder of this tutorial is organized as follows: Section II provides a general overview of the TT&C subsystem, from the architecture to the main design drivers, complemented with a brief survey of actual TT&C subsystems. Then, Section III focuses on the basics of the physical layer of TT&C links, starting with an introduction to the modulation formats, and addressing the details of the three main links (TC, TM, and tracking) along with their sizing. Then, Section IV lays out the fundamentals of the TT&C subsystem "core unit": the transponder. Section V follows, providing an overview of the most recent techniques that could be implemented in future TT&C systems, or that are still open to research. Section VI explains instead the overall standardization framework, highlighting the main applicable standards that are used in this field. Finally, Section VII reviews actual missions that had major TT&C issues, and their lesson learned, while Section VIII draws the conclusions.

II. The TT&C subsystem

The design of a TT&C subsystem is not a standard task. Different space mission objectives and requirements, or simple engineering choices, can lead to completely different configurations. However, this section will show that, despite the unique design of each TT&C subsystem, it is possible to identify some commonalities and underlying rationales in the design. This section will provide an overview of how a TT&C subsystem is typically organized and will explore major design drivers, including frequency allocations, reliability, and other factors. Finally, to reinforce the concepts discussed, a survey of the TT&C subsystems of actual ESA satellites will be provided.

A. Architectures

Figure 2 shows the most basic architecture for a TT&C subsystem: it is composed of two TC receivers, two TM transmitters, two diplexers, and two low gain antennas (LGAs), all interconnected by means of a radio-frequency distribution network (RFDN). The use of two receivers and transmitters is due to redundancy reasons (later discussed in Section II-C). In most cases, the preferred approach is to keep both receivers always ON along the mission. This is commonly referred to as a *hot redundancy* configuration. Differently, only one transmitter is kept ON during transmission periods, while

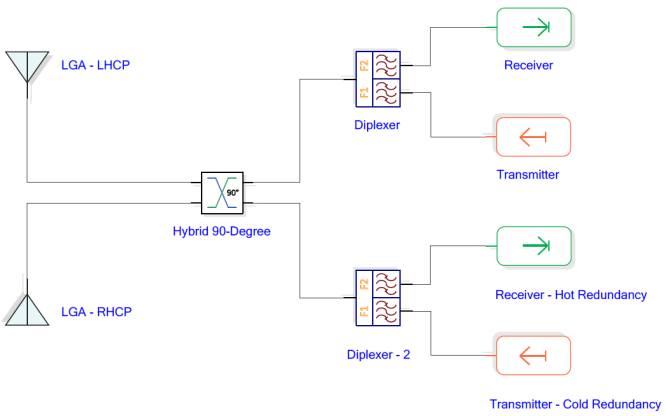

Figure 2. Block diagram of the basic TT&C subsystem architecture.

the other is adopted as a *cold redundancy*. The transmitter and receiver are rarely embarked as separate units. Instead, the two modules are typically integrated into a single unit that also performs the RNG turn-around and is known in "TT&C lingo" as *transponder*. Since TC and TM links work on different frequencies (later described in Section II-B), diplexers are adopted for de-multiplexing the two links from/to the transponder output and input. The diplexer can be either embarked as a separate unit or directly integrated as part of the transponder. The LGAs typically provide wide coverage, with a possible gain of $\geq$ 0 dB in about +/- 90 degrees from boresight. They also use opposite circular polarizations, namely, left and right-hand circular polarization (LHCP and RHCP). Finally, the RFDN is the interconnection between all the aforementioned units and is the ensemble of cables, switches, hybrids, etc. In the example of Figure 2, the RFDN is composed of a 3 dB hybrid that interconnects, using coaxial cables, the diplexer ports with the two LGAs.

It is easy to see that this TT&C subsystem configuration strives to achieve very high reliability: it allows the spacecraft to receive TCs and transmit TM, regardless of the spacecraft's attitude, throughout all the mission phases. In fact, using two LGAs, it achieves an (almost) omni-directional coverage. Adopting LHCP and RHCP ensures that a signal received on a polarization will not cause destructive interference at receiver input (as combinations of the same signal received by both the LGAs). Additionally, the signal transmitted by one of the two transmitters will always excite both antennas, while the signal received by any antenna will be seen at both receiver inputs. Finally, the redundant configuration allows the subsystem to be tolerant to anomalies/malfunctions of one transponder without causing the failure of the whole space mission.

A different approach is usually adopted for the PDT subsystems. The PDT subsystem basic architecture is shown in Figure 3. It is composed of two transmitters in a cold redundancy configuration, while the RFDN interconnects both transmitters to a medium/high gain antenna (MGA/HGA). The figure shows the example of an RFDN composed of a switch with coaxial cables.

The adoption of this configuration is driven by the need of achieving higher bit rates than those achievable by the TT&C

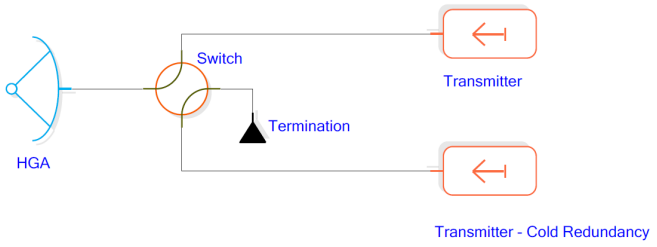

Figure 3. Block diagram of the basic PDT subsystem architecture.

subsystem when the spacecraft is in nominal conditions. Since the higher the bit rate, the higher the equivalent isotropically radiated power (EIRP), the PDT subsystem privileges the use of a switch (rather than a 3 dB hybrid) and an MGA/HGA (instead of LGAs). Even in the case of a failure of one transmitter, the MOC can activate the redundant transmitter chain through dedicated TC to the TT&C.

TT&C and PDT subsystems shall not necessarily be treated as two subsystems. When feasible, it is usual to integrate the PDT transmitter into the TT&C transponder, and a common RFDN is adopted as interconnection with the antennas (LGAs and MGA/HGA). This will be better explained and shown with examples later provided in this paper.

B. *Frequency allocations*

One of the main design drivers for the TT&C and PDT subsystems is the selection of the frequency allocations.

The Radio Regulations of the International Telecommunication Union (ITU/RR, [3]) define the frequency allocations that can be adopted depending on the radio communication service. Most of the TT&C systems usually fall under one of the following services:

- *Earth Exploration Satellite Service* (EESS), that includes Earth Observation (EO) missions (performing meteorological measurements and global monitoring, like *Sentinels* [4]) or space missions that provide information regarding the characteristics of the Earth (like *Smile* mission [5]);
- *Space Research Service* (SRS): applicable to space missions having scientific or technological research purposes. For this service, there is a further distinction between *near Earth* missions and *deep space*, i.e., with distance from Earth less than 2 million km (like *Euclid* or *Ariel*, [6]), or further (like the well-known *Rosetta* mission, or the novel *Solar Orbiter* [7]);
- *Space Operations Service* (SOS): applicable to space missions that exclusively foresee the operation of the spacecraft, i.e., basic TC and TM (e.g., in-orbit servicing vehicles [8]).

Tables I and II provide a summary of the most used frequency allocations for designing Earth-to-Space (TC) and Space-to-Earth (TM) links, namely, S-, X-, K-, and Ka-Band[1]. The TT&C engineer, when designing the subsystem, has to decide which frequency to select for all the possible TT&C and PDT links. This shall be done by considering critical factors such as technology availability and maturity (identified by the so-called TRL [9], [10]), available ground station, and limitations from radio regulations.

At the time of writing, S-Band is the most adopted allocation for TT&C links: it relies on an extensive heritage and, also thanks to a large number of existing ground stations, it often results as the best choice for low-Earth orbit (LEO) missions. However, its popularity is causing non-negligible problems in performing the frequency assignments for future missions, especially those that require large bandwidths. In particular, the 2200-2290 MHz band is one of the most densely occupied bands and ESA missions use (and impose in their requirements) a maximum frequency assignment of 6 MHz [11].

X-Band for SRS (near Earth and deep space) is often selected as a baseline for the TT&C of Science missions, particularly those at Lagrange points or interplanetary missions. The technology development of X-Band units is well mature, and X-Band links are supported by space agencies' ground segment (e.g., the NASA DSN and ESA ESTRACK, [12], [13]). Since Science missions can have a PDT bit rate of about 1-10 Mbps, their PDT subsystem often adopts X-Band. Because of its popularity, similarly to S-Band, ITU imposes for X-Band near Earth a maximum frequency assignment equal to 10 MHz [11].

X-Band for EESS is often selected for PDT links of EO missions. Namely, its large bandwidth allows a bit rate as high as ∼500 Mbps. From Tables I and II, the reader can notice that X-Band for EESS could be adopted also for TT&C links, i.e., the TC link in 7190-7250 MHz and TM link in 8025-8400 MHz. However, at the time of writing, this design has never been adopted yet: the 7190-7250 MHz was opened up for EESS only in 2015 [14], and the technology is still under development.

K-Band will be widely adopted soon as an alternative to X-Band for both SRS and EESS missions. Namely, several EO missions will have PDT bit rates in the order of Gbps, while future Science missions forecast tens/hundreds of Mbps. Since these values cannot fit the X-Band allocations, K-Band PDT subsystems will be implemented. Ka-Band is particularly relevant for deep space missions and serves two main functions: PDT (when bit rates do not fit the available X-Band) and performing radio-science experiments such as RNG measurements that provide specific information about planets' gravity, atmosphere, and more, which cannot be obtained with RNG in X-Band only. With this in mind, Table III summarizes the most common frequency selection choices.

It shall be highlighted that ITU often does not define frequency allocations for all possible space missions, in particular Lunar and Martian, because of its primary interest in

[1]It is pointed out that the nomenclature K- and Ka-Band is not uniform among the engineering domains. In this paper, it is adopted the most common naming used in ESA space missions, i.e., K-Band for ∼27 GHz links, and Ka-Band for ∼32 GHz links.

Table I
FREQUENCY ALLOCATIONS THAT CAN BE ADOPTED FOR EARTH-TO-SPACE TT&C LINKS.

Name	Allocation	Services
S-Band	2025-2110 MHz	SRS (near Earth), SOS, EESS
	2110-2120 MHz	SRS (deep space)
X-Band	7130-7190 MHz	SRS (deep space)
	7190-7235 MHz	SRS (near Earth)
	7190-7250 MHz	EESS

Table II
FREQUENCY ALLOCATIONS THAT CAN BE ADOPTED FOR SPACE-TO-EARTH TT&C LINKS.

Name	Allocation	Services
S-Band	2200-2290 MHz	SRS (near Earth), SOS, EESS
	2290-2300 MHz	SRS (deep space)
X-Band	8025-8400 MHz	EESS
	8400-8450 MHz	SRS (deep space)
	8450-8500 MHz	SRS (near Earth)
K-Band	25.5-27.0 GHz	SRS (near Earth), EESS
Ka-Band	31.8-32.3 GHz	SRS (deep space)

Earth RF interference. This task is covered by the *space frequency coordination group* resolutions and recommendations (SFCG [15], later explained in Section VI-C). Namely, for TT&C systems for Lunar missions, SFCG REC 32-2 applies, while for Martian missions SFCG REC 22-1 applies. These recommendations provide the set of frequencies to be adopted depending on the link direction, such as from/to Earth, orbit-to-orbit, surface-to-orbit, and orbit-to-surface. For the detailed and latest version of the tables, the reader is referred to Table 1 provided in REC 32-2 and 21-1 on the SFCG website [15].

C. Reliability and redundancies

The use of redundancies plays a fundamental role in the reliability of the spacecraft and the whole mission. It is standard to have a backup for any active unit of the subsystem. On the other hand, there are also missions in which no redundancy is adopted or required. For instance, Cubesats can accept a higher risk of failure, and their mission duration can be less than one year. Thus, the redundancy may burden the whole system (by increasing mass, power consumption, or failure modes) rather than being a benefit [16]. To evaluate this trade-off, the

Table III
TYPICAL FREQUENCY ALLOCATION CHOICES FOR EACH KIND OF SPACE MISSION.

Mission type	TT&C	PDT
Earth Observation	S-Band	X-Band, if ∼500 Mbps K-Band otherwise
Science (near Earth	X-Band	as part of TT&C subsystem, if <10 Mbps dedicated K-Band subsystem otherwise
Science (deep space)	X-Band	as part of TT&C subsystem, or dedicated Ka-Band subsystem (if there are radio-science experiments needs)
Space Operations	S-Band	N/A

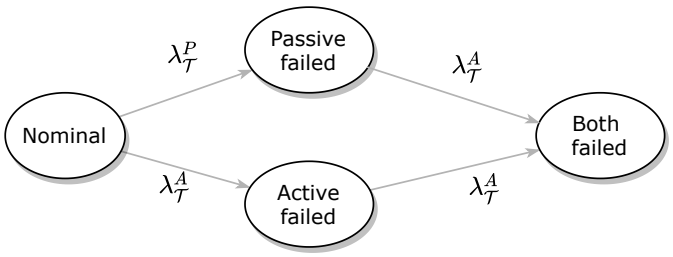

Figure 4. Continous-time Markov chain describing the status of the transponder redundancy scheme of Fig. 2.

system reliability and single point failure analysis is normally carried out throughout the project. Although engineers with dedicated expertise carry out this analysis, the TT&C engineer should be able at least to perform a preliminary assessment to understand whether redundancy is required or not. Thus, this section aims to provide the basics of reliability analysis for the TT&C subsystems.

The lifetime of a generic unit u is modeled using an exponential random variable. This gives the probability of non-failure within the time t as

$$P_u(t) = e^{-\lambda_u t}\,, \tag{1}$$

where λ_u is the average number of failures in time, and thus $1/\lambda_u$ is the average unit lifetime. The factor λ_u is given in units of *failure in time* (FIT), which typically represents the number of failures per 10^9 hours. This value is calculated using reliability data for the individual components within the unit. Since the units have usually different operational modes, with different component derating values [17], the factor λ_u shall be computed as a weighted average among the modes. A common approach for active units is to define the average number of failures in time when the unit is ON ($\lambda_{u,\mathrm{ON}}$) and OFF ($\lambda_{u,\mathrm{OFF}}$), and thus the effective failure rate of the unit reads

$$\lambda_u = \lambda_{u,\mathrm{ON}} d_{\mathrm{ON}} + \lambda_{u,\mathrm{OFF}}(1 - d_{\mathrm{ON}})\,, \tag{2}$$

where $d_{\mathrm{ON}} \in [0, 1]$ is the unit duty cycle.

When redundancy comes into play, the problem becomes more complex. For the sake of clarity, we will refer to the TT&C subsystem example of Figure 2, where there is a redundancy scheme of two transponders (each including one transmitter, one receiver, and one diplexer). However, the concepts here presented can be easily generalized. The transponders have two possible operational modes: one with both receiver and transmitter ON, and the other with the transmitter OFF. Hence, we can define the corresponding failure rates as $\lambda_{\mathcal{T},\mathrm{ON}}$, and $\lambda_{\mathcal{T},\mathrm{OFF}}$ respectively. In turn, the two transponders can be adopted with different duty cycles. One transponder is adopted as an active transponder, i.e., transmitting when required, while the other as a passive (redundant) transponder, receiving only. Using Equation (2), the effective failure rates for the active and the passive transponder are

$$\begin{aligned} \lambda_{\mathcal{T}}^{A} &= \lambda_{\mathcal{T},\mathrm{ON}} d_{\mathrm{ON}} + \lambda_{\mathcal{T},\mathrm{OFF}}(1 - d_{\mathrm{ON}})\,, \\ \lambda_{\mathcal{T}}^{P} &= \lambda_{\mathcal{T},\mathrm{OFF}}\,. \end{aligned}$$

We can now describe the transponder redundancy scheme by means of a continuous-time Markov chain [18] as the one shown in Figure 4. This Markov chain has the following states:

- *nominal*, when both transponders are functional. One transponder is used as the active unit, while the other as the passive one;
- *active failed*, when the active transponder has failed. Thus the passive transponder is activated;
- *passive failed*, when the passive transponder has failed. The active transponder stays as it is;
- *both failed*. Thus, the whole redundancy scheme has failed.

The corresponding Markov chain rate matrix is equal to

$$\boldsymbol{R} = \begin{bmatrix} -\lambda_{\mathcal{T}}^{A} - \lambda_{\mathcal{T}}^{P} & \lambda_{\mathcal{T}}^{A} & \lambda_{\mathcal{T}}^{P} & 0 \\ 0 & -\lambda_{\mathcal{T}}^{A} & 0 & \lambda_{\mathcal{T}}^{A} \\ 0 & 0 & -\lambda_{\mathcal{T}}^{A} & \lambda_{\mathcal{T}}^{A} \\ 0 & 0 & 0 & 0 \end{bmatrix} . \tag{3}$$

Since the redundancy scheme fails when the Markov chain ends in the final state, the probability that this happens during the time t can be computed by means of the Kolmogorov forward equation [18]. The solution of the equation (after some calculations) provides the reliability $P_{\mathcal{T}2}(t)$ of the two transponders as

$$\begin{aligned} P_{\mathcal{T}2}(t) &= 1 - \left[\mathrm{e}^{\boldsymbol{R}t}\right]_{1,4} , \\ &= e^{-\lambda_{\mathcal{T}}^{A} t} \left[1 + \frac{\lambda_{\mathcal{T}}^{A}}{\lambda_{\mathcal{T}}^{P}} \left(1 - e^{-\lambda_{\mathcal{T}}^{P} t}\right)\right] , \end{aligned} \tag{4}$$

where e denotes the matrix exponential, and $[\cdot]_{1,4}$ the entries of the matrix in position (1,4). We are now ready to compute the reliability of the full TT&C subsystem $P_{\mathrm{TT\&C}}(t)$. Since all other units do not adopt any redundancy, the reliability is simply given by

$$P_{\mathrm{TT\&C}}(t) = P_{\mathcal{T}2}(t) P_{\mathrm{RFDN}}(t) P_{\mathrm{LGA}}^{2}(t) , \tag{5}$$

where $P_{\mathrm{RFDN}}(t)$ and $P_{\mathrm{LGA}}(t)$ have expressions as shown in (1). The equation above is often reported in the reliability analysis report using a block diagram as the one shown in Figure 5, which represents redundant units as parallel blocks, and non-redundant ones as serial blocks. Once the λ_u values are defined, Equation (5) can be easily evaluated as a function of time. Typical values for the transponder failure rate are $\lambda_{\mathcal{T},\mathrm{ON}} \sim 1000 - 1500$ and $\lambda_{\mathcal{T},\mathrm{OFF}} \sim 500 - 750$ FIT, while for passive units can be less than 20 FIT.

Figure 6 shows the plot of (5) as function of the time, by using $\lambda_{\mathcal{T},\mathrm{ON}} = 1500$, $\lambda_{\mathcal{T},\mathrm{OFF}} = 500$, $d_{\mathrm{ON}} = 1$, $\lambda_{\mathrm{LGA}} = 14$, and $\lambda_{\mathrm{RFDN}} = 1.55$. For comparison, the figure also shows the reliability in the absence of transponder redundancy, and a typical system requirement of 99% reliability. As expected, the use of redundancy, especially for active units, has a major impact. In the example, the subsystem with transponder redundancy has a reliability of 99% up to ~ 8.5 years. On the other hand, a single transponder could suffice only for missions lasting less than 1 year.

The mathematical framework here presented can be easily generalized to complex TT&C and PDT architectures (like those presented in the following section). In fact, for any set of redundant units, a Markov chain (and its rate matrix) can be defined, and the reliability can be computed numerically by means of Equation (4).

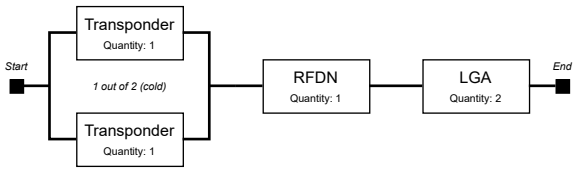

Figure 5. Reliability block diagram of the TT&C subsystem in Figure 2.

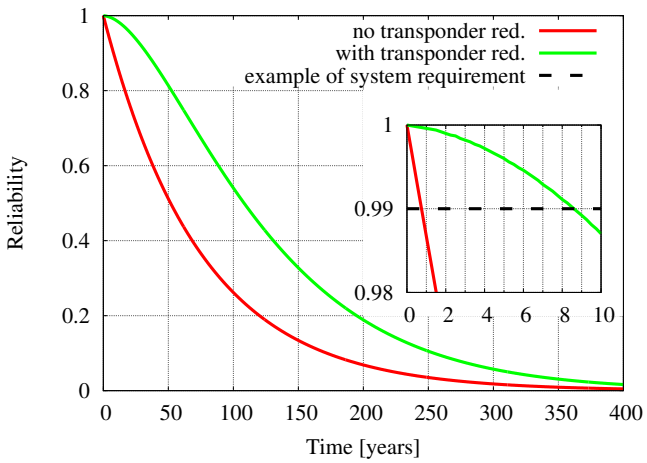

Figure 6. Reliability as function of the time for the TT&C subsystem in Figure 2.

D. Other design drivers

Beyond frequency allocations and reliability, there are several other design drivers to take into account when designing the TT&C subsystem. These can involve rather complex and multidisciplinary problems, thus requiring the TT&C designer to iterate with engineers in other domains. Such design drivers depend on the kind of space mission, science requirements, end-users, operations, technological limitations, and other factors. While it is not possible to cover all of these factors in detail in a single paper, we will focus on the most common ones.

The first fundamental design driver is the *operational concept* of the space mission, usually formalized under the *mission operation concept document* (MOCD), [19]. The concept shall define the operations during the various phases of the mission, including the *launch and early operations phase* (LEOP) and the *nominal* phase [1]. In these phases, the amount of monitoring and autonomous operations are particularly relevant for the TT&C and PDT design. For instance, in LEOP, there are critical operations (such as the propulsions initialization and firing, and attitude stabilization) that are either carried out autonomously by their own subsystems or commanded from the ground. In order for the MOC to maintain regular monitoring of the spacecraft status, it is required a TT&C subsystem with certain characteristics. These include a high bit rate mode (1 Mbps or more) for quick transfer of spacecraft

TM, usage of LGAs without enforcing satellite pointing, and a low bit rate mode with ranging in the event the satellite enters safe mode. In this respect, Sentinel-1A demonstrates how a good TT&C design (which will be described later) played a crucial role during a challenging LEOP [20]. As an additional example, let us consider the nominal phase for a deep space mission. The large distance from Earth allows for only a few bps transmission and reception when using LGAs, which complicates operations. Thus, the TT&C subsystem should always include an HGA for achieving bit rates of some kbps. For more details on the operational concept, the reader can refer to [21].

Another important design driver is the *electro-magnetic compatibility* (EMC) [22]. The TT&C and PDT subsystems, like any other subsystem, shall not cause any harmful interference to the spacecraft's functions. To achieve this, it is necessary to comply with certain requirements of *radiated* and *conducted emissions* (RE, CE), *magnetic moments*, *electrical bonding*, etc [23]. The subsystem shall also withstand its electro-magnetic environment, hence meeting requirements for *radiated* and *conducted susceptibility* (RS, CS), *electro-static discharge*, and other factors that may affect the performance. It should be noted that RS, CS, RE, and CE are interrelated and must be considered together. Specifically, a unit's emissions must be kept lower than the susceptibilities of other units, and vice versa, with a typical margin ratio between the two on the order of 20 dB. In some cases, the EMC requirements can impose stringent constraints on the design of the TT&C subsystem. For instance, the high magnetic moments of the switches may necessitate the adoption of 3 dB hybrids as a substitute. As a consequence, a subsystem like the one in Figure 3, could incur up to a 50% loss of transmitted power in meeting the EMC requirements, resulting in inefficient utilization of resources. For those seeking additional information on EMC, a comprehensive handbook is available at the reference [23].

Finally, *thermal fatigue* has recently emerged as a critical design driver [24]. In general, space units must operate effectively in the environment for which they are designed. This means being able to function within certain limits of shock, vibrations, thermal variations and radiation, without damage or performance degradation. Over time, thermal variations will result in fatigue failure of the constituent unit components. Furthermore, it is becoming increasingly important to consider thermal fatigue due to the ever growing bit rate needs, which result in PDT subsystems requiring higher RF power. This causes large thermal variations that, in turn, limit the maximum number of ON/OFF cycles that the subsystem can perform without damaging the components. This aspect is becoming particularly critical in EO missions, where satellites typically perform one or two PDT switch ON/OFF per orbit, approximately every 0.7-1.5 hours. To mitigate this issue, satellite missions are currently implementing a *mute* function, which removes the RF carrier while keeping the transmitter ON. In this way, it is possible to trade-off the number of mute cycles with the number of switch ON/OFF, staying within the fatigue limits while partially relaxing the thermal control system design.

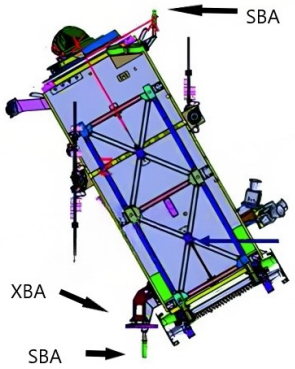

Figure 7. Platform configuration of Sentinel-1, showing the S-Band antennas (SBAs) and the X-Band PDT antenna (XBA). Image credit [27].

E. Review of actual TT&C systems

As already discussed, the TT&C subsystem design widely varies depending on several drivers (the type of mission, bit rates, frequency regulations, reliability needs, etc.). This section shows some examples of actual subsystem architectures, highlighting the rationale behind their design and re-emphasizing the basics discussed in the past sections.

Sentinel-1 ([4], [25]) is an EO satellite operating in a Sun-synchronous orbit around Earth, with an altitude of approximately 690 km. It has a TT&C subsystem in S-Band capable of achieving 64 kbps in TC. As explained in the previous section, it has low and high bit rate mode in TM, of 128 kbps and 2 Mbps, respectively. Its PDT subsystem is in X-Band (EESS), and capable of transmitting at 560 Mbps. The TT&C subsystem consists of two (low-gain) *helix antennas* and two transponders with one diplexer each, exactly as the basic TT&C architecture in Figure 2. As depicted in Figure 7, the two LGAs are positioned on opposing sides of the spacecraft, with one facing the Earth's direction and the other facing the zenith. The LGAs have opposite circular polarizations, resulting in an omni-directional coverage.

Instead, Figure 8 shows the Sentinel-1 PDT subsystem transmitting at 560 Mbps. However, a single transmitter could not support such a high bit rate. Differently from the basic scheme of Figure 3, the TT&C subsystem was designed with two transmitting chains, each capable of transmitting up to 280 Mbps. Each chain consists of a nominal transmitter, a redundant one, and traveling wave tube amplifiers (TWTAs) as external high power amplifiers. The two transmitting chain signals are then multiplexed using an output multiplex filter (OMUX). The PDT antenna, an *isoflux* [26], is mounted to face the Earth direction, as depicted in Figure 7. Its beam shape is designed to guarantee that the signal strength, as seen from Earth, remains nearly constant regardless of the satellite's angle of view, and with no need for an on-board steering of the antenna.

Euclid [28] is a near Earth Science mission that will operate in a large amplitude orbit around the second Sun-Earth Lagrange point (SEL2), with a distance from Earth up to $\sim$1.8 million km. Euclid's TT&C subsystem is in X-Band (SRS near

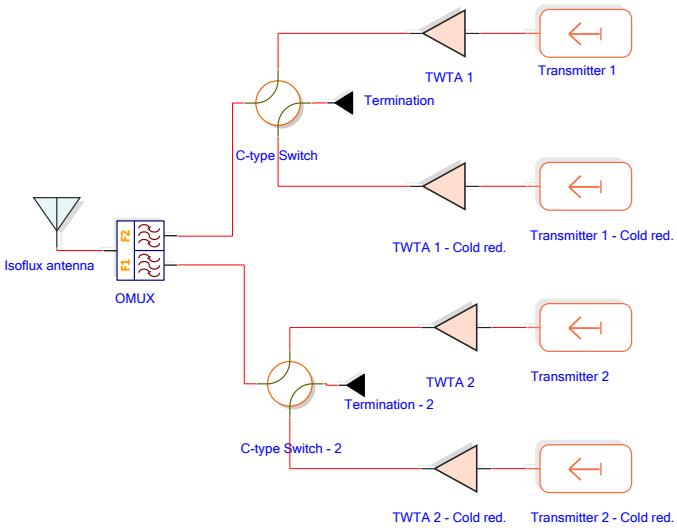

Figure 8. Block diagram of the PDT subsystem of Sentinel-1 (see [25]).

Earth), able to support TC and TM links in the order of some kbps, and its block diagram is shown in Figure 9. The TT&C subsystem adopts a scheme with transponder redundancy and two helix antennas, LGA-1 and LGA-2, with opposite polarizations. These were mounted as shown in Figure 10 for providing an (almost) omni-directional coverage. Differently from the basic TT&C subsystem architecture of Figure 2, a third antenna (LGA-3) was included: mounted on an antenna pointing mechanism (on top of the HGA, later explained) that always points to Earth during nominal phases. Hence, depending on C-type switch-2 position (as shown in the block diagram), the spacecraft can use the LGA-3 for having higher TC and TM bit rates during nominal phases, or LGA-1 and 2 when in need of an omni-directional pattern. For achieving the required EIRP, TWTAs are adopted as external power amplifiers and interconnected to the diplexers by means of a second C-type switch that, in turn, provides a cross-strapping with all the LGAs. Finally, 3-dB hybrids are adopted for cross-strapping receivers and transmitters with the diplexers and TWTAs, respectively. The Euclid PDT subsystem, shown in Figure 11, is instead composed of one HGA and two redundant transmitter chains. The only difference w.r.t. the basic PDT architecture of Figure 3 is the presence of TWTAs that are cross-strapped with the transmitters by means of a 3 dB hybrid.

III. TT&C LINKS

After having discussed the TT&C from a subsystem perspective, this section aims to provide the basics of its physical layer. TT&C links are designed according to the standards dictated by the *consultative committee for space data systems* (CCSDS) and, for European missions (including ESA), also to those of the *European cooperation for space standardization* (ECSS), later described in Section VI. For the sake of clarity, since the standards are very similar, we will refer in the following sections to ECSS standards. However, the reader can find some of the major differences between the two standards in Section VI-B.

It is also pointed out that the classical TT&C nomenclature, as shown in Figure 12, is adopted. The word *bit* means the useful unit of information, whereas *symbols* are the bits after encoding. In the case of SP-L modulation (later explained), rates are expressed in terms of *equivalent symbols* that are nothing else than half of a symbol. Modulation symbols are denoted as *channel symbol*. While rates for bits are expressed using the classical *bps* unit, to complicate things, TT&C engineers usually adopt the symbol per second unit *sps* for symbols, equivalent symbols, and channel symbols. Hence, the reader is recommended to always pay special attention to the type of symbols in question.

The remainder of this section is organized as follows. First, Section III-A describes the RF modulations adopted in TT&C and their spectral properties. Then, Sections III-B and III-C provide a detailed description of the physical layer for TC and TM, explaining how to use a specific modulation and coding format for each kind of satellite mission. Additionally, they include discussions about performance, advantages, and disadvantages. Sections III-D and III-E describe the waveform adopted for ranging links and how the ranging signal combines with TC and TM data communications. Finally, Section III-F defines the link sizing (the link budget) for satellite missions, showing a small example as a tutorial exercise.

A. RF modulations

In TT&C there are basically two families of RF modulations: *residual carrier* and *suppressed carrier* [29]. Suppressed carrier modulations are classical linear modulations as BPSK, QPSK, OQPSK, 8PSK, and amplitude PSK (APSK, [30]), for which group of bits/symbols are mapped into specific channel symbols. On top of these, the well-known GMSK modulation [31] can be also adopted. Being this kind of modulation well-known, they will not be treated in this paper. For further detail on the constellation formats, mapping, and other aspects adopted in TT&C, the reader can refer to [32], [33]. In contrast, residual carrier modulations in TT&C are not widely used in other telecommunications fields, and therefore, this section will provide a detailed discussion on this topic. As the name suggests, residual carrier modulation is a format that keeps a portion of the carrier tone instead of using all the available power to transmit information. The advantage of adopting this old-fashioned signal format is that the residual carrier acts as a "permanent pilot" that can aid in acquisition and synchronization, especially at low signal-to-noise ratios (SNRs). The complex base-band mathematical expression, normalized in power, of a residual carrier modulation is a phase modulation (PM) in the form

$$s(t) = e^{jm_{\mathrm{x}}x(t)}\,, \tag{6}$$

where m_{x} is the modulation index and $x(t)$ is the modulating signal. In most of the ESA satellite missions, the modulating

This article has been accepted for publication in IEEE Communications Surveys & Tutorials. This is the author's version which has not been fully edited and content may change prior to final publication. Citation information: DOI 10.1109/COMST.2023.3287431

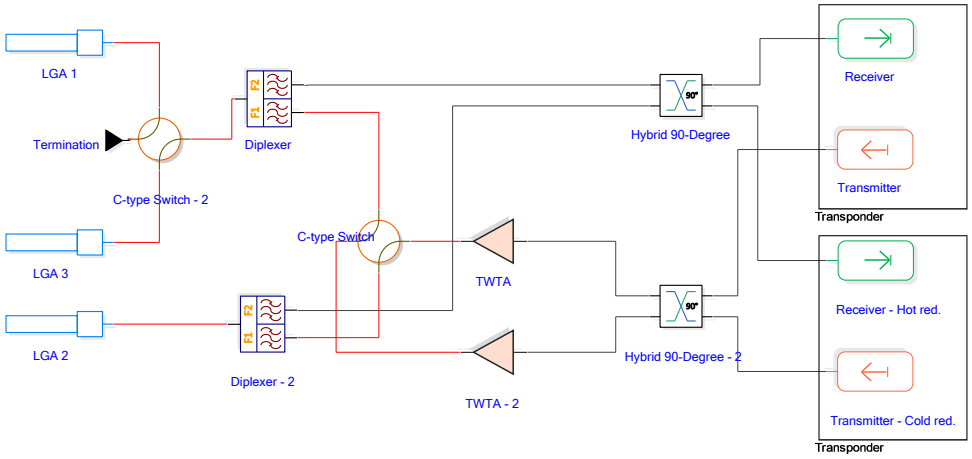

Figure 9. Block diagram of the TT&C subsystem of Euclid (see [28]).

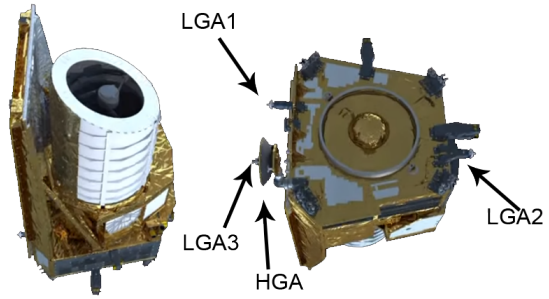

Figure 10. Euclid satellite configuration, as seen from above (left) and below (right), and showing the three X-Band LGAs and the K-Band HGA.

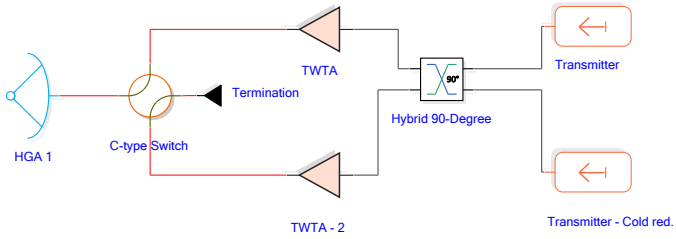

Figure 11. Block diagram of the PDT subsystem of Euclid (see [28]).

signal $x(t)$ can be a binary non-return-to-zero signal with sub-carrier (NRZ/BPSK), or, split-level (SP-L).

The NRZ/BPSK signal reads

$$x(t) = \sum_k a_k p(t - kT) \sin(2\pi f_{\mathrm{x}} t)\,, \tag{7}$$

where T is the channel symbol time, $p(t) = \mathrm{rect}(t/T)$ is a rectangular shaping pulse, $a_k \in \{\pm 1\}$ are binary channel symbols, and f_{x} is the sub-carrier frequency. Plugging (7) into (6), the transmitted signal reads

$$s(t) = e^{j m_{\mathrm{x}} \sum_k a_k p(t-kT) \sin(2\pi f_{\mathrm{x}} t)}\,,$$

and a PM NRZ/BPSK signal (NRZ/BPSK/PM) is obtained. Although the full expression of the NRZ/BPSK/PM signal can appear cumbersome, it has a simple approximation. In fact, using the Jacobi-Anger identity [34], $s(t)$ can be rewritten as

$$s(t) = \sum_i \mathrm{J}_i \left(m_{\mathrm{x}} \sum_k a_k p(t - kT) \right) e^{j2\pi i f_{\mathrm{x}} t}\,,$$

where $\mathrm{J}_i(\cdot)$ is the modified Bessel function of the first kind. Taking into account that $\mathrm{J}_i(m_{\mathrm{x}}) \to 0$ for $i \to \infty$, it can be shown that the signal is well approximated by the expression

$$s(t) \approx \mathrm{J}_0(m_{\mathrm{x}}) + 2j\mathrm{J}_1(m_{\mathrm{x}}) \sum_k a_k p(t - kT) \sin(2\pi f_{\mathrm{x}} t)\,. \tag{8}$$

From this equation it can be observed that $s(t)$ is composed of a residual carrier that keeps a fraction equal to $\mathrm{J}_0(m_{\mathrm{x}})^2$ of the total signal power, while only $2\mathrm{J}_1(m_{\mathrm{x}})^2$ is used to transmit data over the sub-carrier.

Differently, an SP-L signal reads

$$x(t) = \sum_k a_k p(t - kT)\,, \tag{9}$$

where $p(t) = \mathrm{rect}\left((2t - T/2)/T\right) - \mathrm{rect}\left((2t + T/2)/T\right)$ is a Manchester encoded shaping pulse. Since Manchester encoding has two rising edges per symbol time T, the equivalent symbol time (as explained in Figure 12) is equal to $T/2$. Plugging (9) into (6), a PM SP-L signal (SP-L/PM) is obtained and, by using Euler's formula, it reads

$$s(t) = \cos(m_{\mathrm{x}}) + j \sin(m_{\mathrm{x}}) \sum_k a_k p(t - kT)\,. \tag{10}$$

From the equation, it is easy to see that the SP-L/PM signal has a residual carrier with power a fraction equal to $\cos(m_{\mathrm{x}})^2$, while only $\sin(m_{\mathrm{x}})^2$ is used for data transmission.

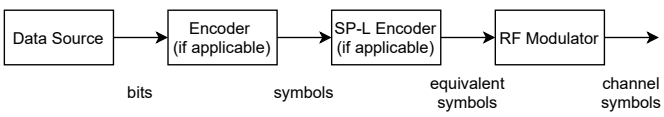

Figure 12. TT&C nomenclature for bits, symbols, equivalent symbols, and channel symbols.

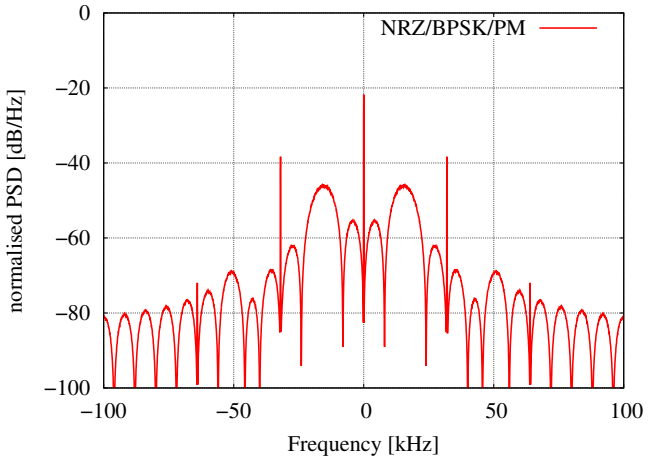

Figure 13. Normalized PSD for a NRZ/BPSK/PM signal, modulation index $m_{\mathrm{x}} = 1.0$ rad/peak, channel symbol rate $1/T = 8$ ksps, and sub-carrier frequency $f_{\mathrm{x}} = 16$ kHz.

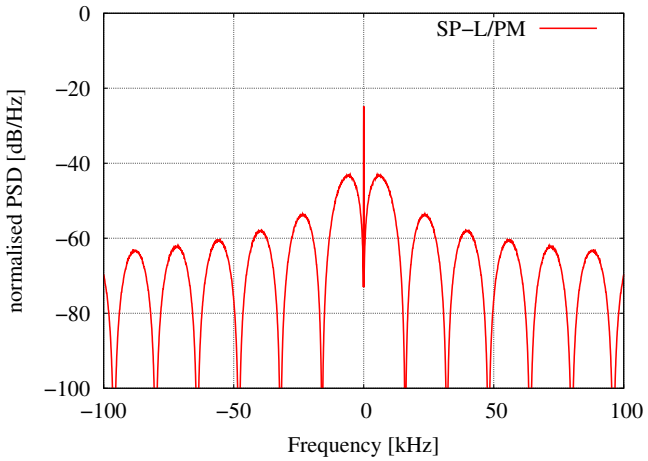

Figure 14. Normalized PSD for a SP-L/PM signal, modulation index $m_{\mathrm{x}} = 1.0$ rad/peak, and channel symbol rate $1/T = 8$ ksps.

Figures 13 and 14 show the simulated spectra of a NRZ/BPSK/PM and of an SP-L/PM signal, with a resolution bandwidth R_{BW} of 58.6 Hz. Both signals have modulation index $m_{\mathrm{x}} = 1.0$ rad/peak and channel symbol rate $1/T$ equal to 8 ksps. In the case of NRZ/BPSK/PM signal, a sub-carrier with $f_{\mathrm{x}} = 16$ kHz was adopted. In agreement with the mathematical equations derived in (8) and (10), the residual carrier has a normalized power spectral density (PSD) equal to $\mathrm{J}_0(m_{\mathrm{x}})^2/R_{\mathrm{BW}}$ and $\cos(m_{\mathrm{x}})^2/R_{\mathrm{BW}}$, respectively. Additionally, it is worth noting that the main lobes (corresponding to the information signal) in the case of NRZ/BPSK/PM are located at $f_{\mathrm{x}} = \pm 16$ kHz. Whereas, for SP-L/PM. they are centered around $1/T = \pm 8$ kHz. By means of (8) and (10), it can be shown that the normalized PSD for these lobes is equal to $T\mathrm{J}_1(m_{\mathrm{x}})^2$ and (about) $T\sin(m_{\mathrm{x}})^2/2$.

RF modulations have several requirements to be compliant, set by both the CCSDS and ECSS. These requirements cover several aspects such as maximum occupied bandwidth, spectral masks, maximum power flux density on Earth's surface, modulation linearity, frequency stability, and many others. As these requirements can vary depending on specific mission needs, they cannot be fully listed here. For a more comprehensive (but not complete) overview, the reader can refer to the ECSS standard in [11].

B. TC links

TC links for space missions are usually designed in compliance with the requirements dictated by the ECSS specifying modulation, synchronization, and channel coding as provided in [11], [35].

The TC link shall reliably transmit low data rate commands from the ground to ensure their execution by the spacecraft. Thus, according to these standards, the TC physical layer shall adopt residual carrier modulations and a discrete set of symbol rates. Namely, the TC link can have a symbol rate multiple or sub-multiple of 4000 sps with respect to a factor of 2^n. The minimum and maximum rates are 7.8125 sps and 256 ksps, respectively. Additionally, depending on the chosen symbol rate, the TC modulation has to comply with the cases reported in Table IV: for rates between 7.8125 and 4000 sps, the TC signal shall be NRZ/BPSK/PM, while SP-L/PM otherwise. Furthermore, the NRZ/BPSK/PM shall have a sinusoidal sub-carrier having a frequency f_{x} equal to 8 or 16 kHz, and a modulation index ranging from 0.2 to 1.4 rad/peak. Differently, for SP-L/PM, no sub-carrier shall be adopted, and the modulation index shall be between 0.2 and 1.0 rad/peak.

The TC coding and synchronization layer foresees the use of a Bose–Chaudhuri–Hocquenghem (BCH) code [36] or low-density parity-check code (LDPC) [37]. For the sake of clarity, this section will only discuss the BCH case, which was the sole coding scheme available for satellite missions until 2021. The topic of LDPC will be tackled in Section V. The BCH for TC, usually denoted as BCH(63,56), encodes 56 bits into a codeword of 63 bits, plus an additional 0 bit as filling (thus making a total codeword length of 64 bits). The full specification of this code and its encoding procedure can be found in [38]. However, it is important to highlight that the BCH in question can be either adopted in a triple-error detection (TED) mode or in a double-error detection mode with single error correction (SEC). ECSS in [35] recommends to use the latter only. As shown in Figure 15, the TC frame (coming from the data link layer [39]) is sliced into blocks of 56 bits[2] and randomized by means of an XOR with a specific pseudo-random sequence defined by the standard. These blocks are then BCH encoded into a 64-bit codeword, finally forming a BCH *codeblock*[3]. At last, a *communication link transmission unit* (CLTU) is constructed by adding a 16-bits start sequence and a 64-bits tail sequence. The start sequence, expressed in hexadecimal, reads 0xEB90: this specific bit pattern has good autocorrelation properties that allow to synchronize the start of a CLTU and delimit the beginning of the first codeword. Differently, the tail sequence reads 0xC5C5...C579, and it is

[2]In case the TC frame is not a multiple of 56 bits, then a *filling* is performed by appending the sequence 0101... to the TC frame until the TC frame has the number of bits required.

[3]For the reader's convenience, it is pointed out that, in this paper, we refer to a codeblock as a group of codewords.

Table IV
TC SYMBOL RATES, MODULATIONS (WITH USE OF SUB-CARRIERS), AND ENCODING, ACCORDING TO ECSS STANDARDS.

Symbol rate	Modulation	Sub-carrier f_{x}	Sub-carrier waveform	Modulation index m_{x}	Encoding
$4000\ /2^n$ $n = 0, ..., 9$	NRZ/PSK/PM	8 or 16 kHz	$\sin(\cdot)$	0.2 - 1.4 rad/peak	BCH or LDPC
$4000\ \cdot 2^n$ $n = 1, ..., 6$	SP-L/PM	N/A	N/A	0.2 - 1.0 rad/peak	BCH or LDPC

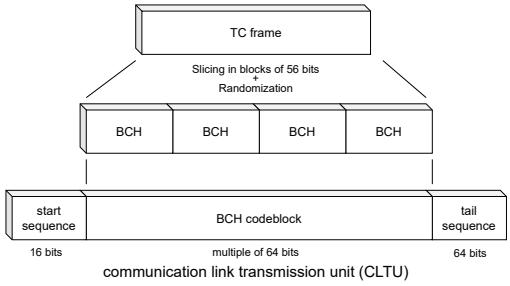

Figure 15. Encapsulation of a TC frame into a CLTU.

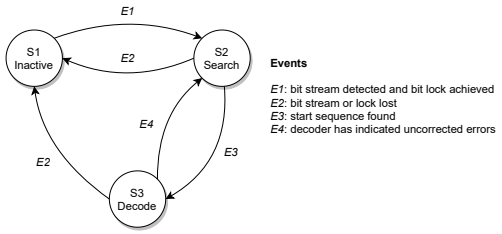

Figure 16. State diagram for the TC receiver.

a specific pattern constructed to be *non-correctable*[4] by the BCH(63,56) decoder (with a rationale later explained).

The CLTUs' transmission follows a specific procedure, known as *physical layer operation procedure 2* (PLOP-2)[5], based on a specific receiving logic. The TC receiver must be designed by implementing the state diagram shown in Figure 16. According to the figure, the receiver starts in an *Inactive* state, waiting to detect a bit stream and achieve the bit lock (*E1* event). After the event, the receiver moves into a *search* state that looks for the CLTU starting sequence (*E3*). Once found, decoding can be initiated. During decoding, when non-correctable errors are found (*E4*), the receiver goes back to the search state. In case the link is lost at any time (event *E2*), the receiver returns to the inactive state. In light of this reception logic, PLOP-2 follows the process in Figure 17. The TC session starts with an unmodulated carrier followed by a TC signal with a 128-bit acquisition sequence (different from the CLTU start sequence) consisting of alternating bits of 1 and 0. This sequence triggers the receiver to move into the search state. At this stage, CLTUs are transmitted, each separated with an 8-bit idle sequence of alternating bits of 1 and 0. At the end of each CLTU, the tail sequence causes the BCH decoder at the receiving end to reject the codeword (event *E4*). Thus, for each transmitted CLTU, the receiver alternates between the decode and search states. Finally, at the end of the TC session (when there are no more CLTUs to be transmitted), the signal is removed by forcing the receiver to go back to the inactive state (event *E2*). Optionally, at points a) and b) of Figure 17, a mission can introduce an idle sequence and an unmodulated carrier step, respectively.

[4]In this paper and the TC standards, a non-correctable pattern is a sequence for which the decoder can declare uncorrected errors. This definition is valid for a BCH decoder either in TED or SEC mode.

[5]Beyond PLOP-2, TC standards also foresee the use of the former PLOP-1, that shall be adopted exclusively for legacy missions. The full description of PLOP-1 can be found in [35].

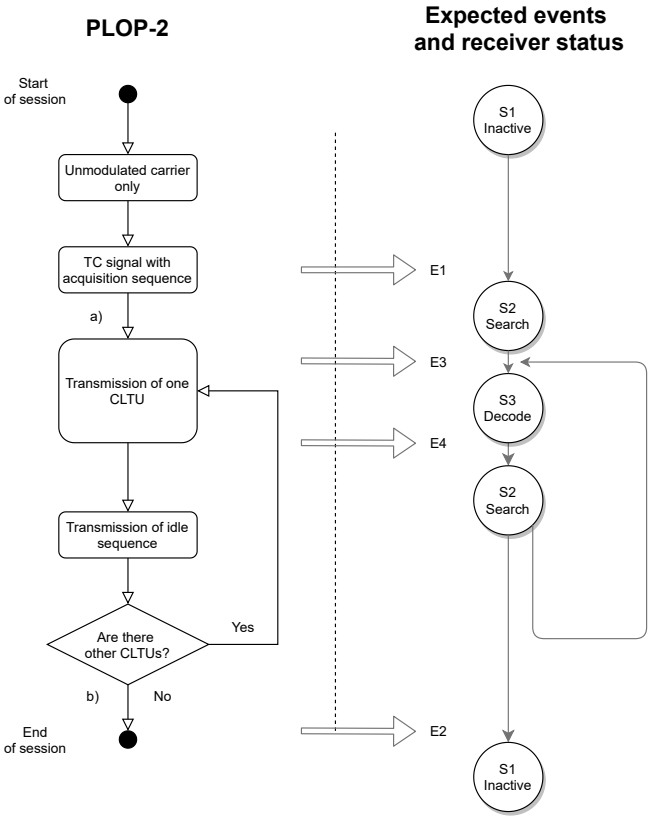

Figure 17. Flow diagram of PLOP-2 and expected events and receiver status for the correct reception of CLTUs during a TC session.

While the CLTU tail sequence serves as a non-correctable BCH codeword for detecting the end of the CLTU, it is susceptible to standard bit or synchronization errors that can cause premature termination of the CLTU and rejection of the entire TC frame at the upper layer. Moreover, a missed error detection could cause undetected errors in the TC frame. We will now lay down the basics for estimating the probability of *TC frame rejection* and *undetected errors in a TC frame*. We assume the use of BCH(63,56) hard-decoding with SEC, and accept the start sequence with a maximum of one error, as specified by ECSS by ECSS [35]. For the complete mathematical details and the case of BCH hard-decoding with TED, the reader can refer to [40].

Since PLOP-2 starts with an unmodulated carrier and a 128-bit acquisition sequence (possibly extended by the idle sequence), the probability of missed bit detection and bit lock can be considered negligible. Thus, the main events that contribute to the incorrect CLTU rejection probability are: *start sequence not recognized*, *BCH codeblock rejected*, *tail sequence is missed*. The probability of not recognizing the start sequence, denoted as P_{start}, can be calculated as the probability of having two or more errors in the 16-bit sequence. Namely,

$$P_{\text{start}} = 1 - (1-P_b)^{16} - \binom{16}{1} P_b (1-P_b)^{15}\,, \qquad (11)$$

where P_b is the bit error rate. Differently, the probability P_{BCH} that a BCH codeblock is rejected can be quite cumbersome to compute. In fact, the codeblock is rejected if errors are detected in any of the BCH codewords. But, two or more errors (depending on their number and if they are even/odd) can still make the BCH decoder declare (mistakenly) the codeword valid. Luckily, these events are negligible in the overall probability calculation. Thus the probability P_{BCH} can be upper-bounded with good precision [40] as

$$P_{\text{BCH}} \leq 1 - \left[(1-P_b)^{63} + \binom{63}{1} P_b (1-P_b)^{62} \right]^{N_{\text{BCH}}}\,, \qquad (12)$$

where N_{BCH} is the number of BCH codewords per CLTU. Finally, the probability P_{tail} of missing the tail sequence is given by the probability that the tail sequence is a valid codeword. It can be shown that there are 1953 and 651 combinations of two and three errors, respectively, that contribute to such a probability, while other terms are negligible [40]. As a consequence, the probability of missed tail sequence can be upper-bounded as

$$P_{\text{tail}} \leq 1953 \cdot P_b^2 (1-P_b)^{61} + 651 \cdot P_b^3 (1-P_b)^{60}\,. \qquad (13)$$

We are now ready to compute the TC frame rejection rate and the probability of undetected errors. For the former, by considering that the CLTU contains a single TC frame, the probability of rejection $P_{\text{TC},rej}$ is given by (14). Namely, the frame is rejected if, in chronological order, the tail sequence of the previous CLTU is missed, the start sequence is not recognized, or the BCH codeblock is rejected. Similarly, using the approach of previous equations, the probability of undetected errors $P_{\text{TC},und}$ can be found. The technical report [40] showed, by means numerical simulations, that the main contributors to the undetected errors probability are 39060 and 9765 codewords of three and four errors, respectively. Thus, $P_{\text{TC},und}$ is well approximated by means of (15).

Figure 18 shows $P_{\text{TC},rej}$ and $P_{\text{TC},und}$ as functions of the energy-per-bit over noise spectral density E_b/N_0 for the AWGN channel (for which it holds $P_b = Q(\sqrt{2E_b/N_0})$). The probabilities are shown for N_{BCH} equal to 10 and 50. It can be seen that as N_{BCH} increases, the rejection and undetected errors probability increase. This behavior is also visible in Figure 19, which shows the probabilities as functions of N_{BCH} for different values of P_b. Therefore, if the mission imposes maximum aloowable values for $P_{\text{TC},rej}$ and $P_{\text{TC},und}$, P_b and N_{BCH} shall be properly sized.

As an example, let us consider that the mission requirements impose $P_{\text{TC},rej} \leq 10^{-3}$ and $P_{\text{TC},und} \leq 10^{-9}$, which are typical values for space missions [40]. Additionally, let us assume that $P_b = 10^{-5}$, as recommended by ECSS communication standard [41]. By looking at the figures, we can see that these requirements are met if $N_{BCH} \lessapprox 50$, while for larger codeblocks, $P_{\text{TC},und}$ increases to around 10^{-8}. Thus, if $N_{\text{BCH}} \geq 50$ is needed, the designer should decrease P_b accordingly to meet the requirements.

In reality, space missions can also resort to another alternative: TC frames can include a 16-bit cyclic redundancy check (CRC), as described in [42]. If the CRC is implemented, $P_{\text{TC},und}$ can decrease by several order of magnitude (e.g., from 10^{-8} down to 10^{-18}), without affecting $P_{\text{TC},rej}$. This comes at the price of a small overhead in the TC frame and additional hardware complexity in the spacecraft receiving system. For further details, the reader can refer to [40], Section 9.5.

C. TM links

TM links are designed in compliance with the requirements dictated by ECSS concerning modulation, synchronization, and channel coding, as provided in [11] and [43].

Table V shows a summary of the modulation schemes that can be adopted for the TM physical layer. As the table shows, the TM signal can be either a residual or a suppressed carrier modulation, depending on the target symbol rate and type of mission. Residual carrier modulations are typically used for critical operations, such as a spacecraft in emergency mode, where low TM rates are required. On the other hand, nominal operations use high rates, and to maximize spectral efficiency (which is often a concern), suppressed carrier modulations (possibly filtered) are adopted. Standards dictate that for rates below 60 ksps, an NRZ/PSK/PM scheme can be used, with either a sinusoidal or squared sub-carrier depending on whether the mission is near Earth or deep space[6]. Differently, SP-L/PM can be used for rates between 10-1000 ksps. However, based on the authors' personal experience, it is not recommended to use a rate higher than 128 ksps to ensure compliance with the bandwidth and spectral requirements outlined in Section III-A.

[6]The squared sub-carrier is obtained by replacing the term $\sin(2\pi f_{\text{x}} t)$ in Equation (7) with $\sum_k (-1)^k \text{rect}(2f_{\text{x}} t - k)$, where $\text{rect}(\cdot)$ a unitary squared pulse in $[-0.5, 0.5]$.

$$P_{\mathrm{TC},rej} \approx P_{\mathrm{tail}} + (1 - P_{\mathrm{tail}}) \left[P_{\mathrm{start}} + (1 - P_{\mathrm{start}}) P_{\mathrm{BCH}} \right] \quad (14)$$

$$P_{\mathrm{TC},und} \approx 1 - \left[1 - 39060 \cdot P_b^3 (1 - P_b)^{60} - 9765 \cdot P_b^4 (1 - P_b)^{59} \right]^{N_{\mathrm{BCH}}} \quad (15)$$

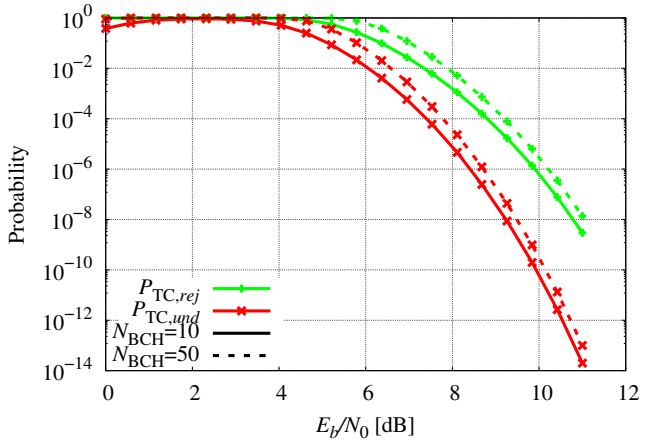

Figure 18. Probability of TC rejection rate $P_{\mathrm{TC},rej}$ and of undetected errors $P_{\mathrm{TC},und}$ as function of E_b/N_0.

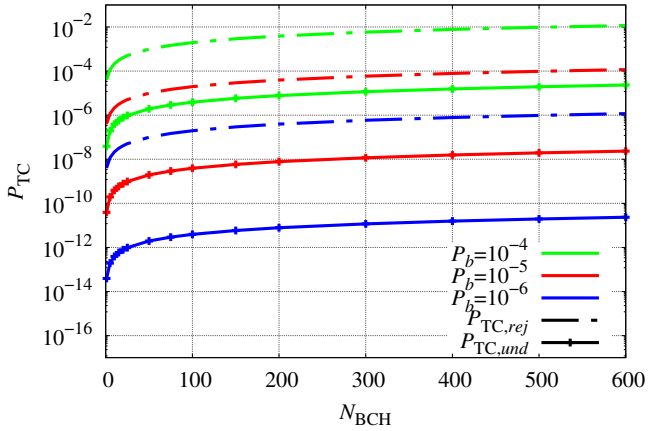

Figure 19. Probability of TC rejection rate $P_{\mathrm{TC},rej}$, and undetected errors $P_{\mathrm{TC},und}$ in the CLTU, as function of the number of BCH codewords per codeblock.

Finally, as reported in Table VI, for any other data rate, suppressed carrier modulations can be adopted. The designer should take into account the following points:

- suppressed carrier modulations at low symbol rates (and thus operating at low SNR) can have synchronization issues. Hence, in the authors' experience, it is recommended to use suppressed carrier modulations only when the symbol rate is roughly higher than 1 Msps;
- Modulations as BPSK, QPSK, Unbalanced-QPSK (UQPSK), Offset-QPSK (OQPSK) are defined as direct modulation of an NRZ symbol stream (see [11], Section 6.2.3), hence with spectra resembling a $\mathrm{sinc}(\cdot)$. Since these modulations are not spectrally efficient, ECSS [11] enforces to adopt them only for symbol rates ≤ 2 Msps for links in S- and X-Band, and ≤ 20 Msps for links in Ka-Band;
- Filtered OQPSK is obtained by using a squared-root raised cosine (SRRC) filter, having a roll-off of 0.5 or an elliptic filter. Similarly, TCM-8PSK, can adopt SRRC with a roll-off of 0.35 or 0.5, or an elliptic filter;
- GMSK has a spectral efficiency driven by the parameter BT, i.e., the product of the one-sided 3-dB Gaussian filter bandwidth with the symbol time. This parameter shall be chosen as a trade-off between spectral efficiency and demodulation loss. Namely, as BT decreases, the spectral efficiency increases, but inter-symbol interference (ISI) at the receiver also increases. Differently, as BT increases, both spectral efficiency and ISI decrease. For this reason, it is recommended that near Earth missions, usually band-limited, implement GMSK with $BT = 0.25$. Whereas, deep space missions, typically power limited, use GMSK with $BT = 0.5$ [32];
- 8PSK trellis code modulation (8PSK-TCM) can be implemented either with a spectral efficiency factor (SEF) of 2 symbols/channel symbols, or, 2.5 symbols/channel symbols.

The TM synchronization and coding layer foresees the use of different coding schemes that can be applied at two different levels: at the TM transfer frame or *channel access data unit* (CADU) level (later defined). Table VII and VIII show the full list of coding techniques at these two levels, namely, Convolutional coding (CC, possibly punctured), Reed-Solomon (RS), Turbo codes, and LDPC. For the complete implementation details of these coding schemes, the reader can refer to the document [44].

TM frames can be encoded following two possible logic schemes: one specific for LDPC at the CADU level (as by Table VIII), and one adopted in all the other cases. The latter is shown in Figure 20. TM frames (coming from the data link layer [45]) are provided with an *attached synch marker* (ASM), a specific bit pattern that aids the frame synchronization at the receiving end, and followed by the forward error correction (FEC) bits of one of the coding schemes in Table VII. The resulting frame, known as CADU, can be optionally randomized (except for its ASM) by means of an XOR with a specific pseudo-random sequence, as defined in [44]. In the only case of TM frames that are RS encoded or uncoded, then the stream of CADUs can be convolutionally encoded. The combination of RS with CC is known as *concatenated*.

Differently, when the LDPC in Table VIII is adopted, the logic scheme to be used is shown in Figure 21: a stream of synch-marked TM frames are asynchronously sliced into information blocks that, in turn, are LDPC encoded. Since the

Table V
TM SYMBOL RATES, MODULATIONS (WITH USE OF SUB-CARRIERS), AND ENCODING, ACCORDING TO ECSS STANDARDS.

Symbol rate	Modulation	Sub-carrier f_{x}	Sub-carrier waveform	Modulation index m_{x}	Encoding
$0.1 - 60$ ksps	NRZ/PSK/PM	2-300 kHz and multiple of symbol rate$^{(*)}$	$\sin(\cdot)$, if near Earth $\sum \mathrm{rect}(\cdot)$, if deep space	≤ 1.5 rad/peak, if near Earth ≤ 1.25 rad/peak, if deep space	see Table VII
$10 - 1000$ ksps (recommended ≤ 128 ksps)	SP-L/PM	N/A	N/A	≤ 1.25 rad/peak	see Table VII
any if filtered, limited to values in Table VI if unfiltered, (recommended ≥ 1 Msps)	Suppressed carrier see Table VI	N/A	N/A	N/A	see Table VII

$^{(*)}$ for sub-carrier frequency higher than 60 kHz, the frequency to symbol rate ratio shall not exceed 4 for near Earth missions, and 5 for deep space missions..

Table VI
LIST OF ALLOWABLE TM SUPPRESSED CARRIER MODULATIONS.

Suppressed carrier modulation
BPSK$^{(*)}$
QPSK$^{(*)}$
UQPSK$^{(*)}$
OQPSK$^{(*)}$
Filtered OQPSK
GMSK
8PSK-TCM

$^{(*)}$ only for symbol rates ≤ 2 Msps in S- and X-Band, and, for symbol rates ≤ 20 Msps in Ka-Band (as defined in Table II).

Table VII
LIST OF ALLOWABLE TM CHANNEL CODES AT TM FRAME LEVEL.

Code	Rate
RS	223/255
RS (for 8PSK-TCM)	239/255
Turbo	1/6, 1/4, 1/3, 1/2
LDPC	1/2, 2/3, 4/5, 223/255 ($\sim$7/8)

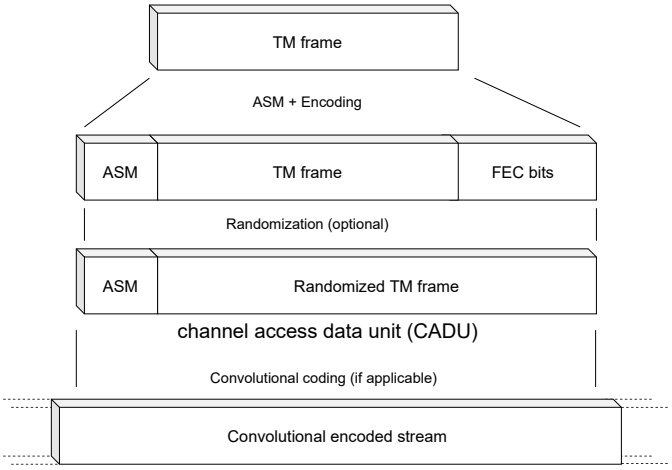

Figure 20. Encapsulation of a TM frame into a CADU. In case the TM frame is uncoded or RS encoded, it can be further protected with application of CC at CADU level.

ASM cannot be employed anymore for frame synchronization, the resulting LDPC codewords are grouped into blocks with attached a new marker, known as *code synch marker* (CSM). Each LDPC codeblock is composed by a (mission specific) fixed number of LDPC codewords. Consequently, for this case, the CADU is the composition of the CSM and LDPC codeblock.

As the reader can notice, the TM link can be designed with different combinations of modulation and coding formats that have been expanding over time, following technical advances in the field, while keeping several technology features that justified their inclusion in the TM standards. However, in practice, missions resort only to a few cases. A summary of the most frequent design combinations, adopted in ESA missions, is shown in Table IX. In particular:

- EO missions typically have TT&C links with bit rates targeting 100-3000 ksps, thus resorting to SP-L/PM or OQPSK. These missions, because of their proximity to Earth, often have links with an SNR that is high enough to require only a moderate coding rate and gain. Thus, it is typical to adopt an RS or concatenated coding approach. Differently, their PDT usually targets hundreds of Mbps, taking the whole available bandwidth while maximizing as much as possible the spectral efficiency. For this reason, the EO PDT link usually resort to 8PSK-TCM (with SEF equal to 2.5) combined with RS 239/255, thus with a total efficiency of about 2.3 bits per channel symbol;
- near Earth Science missions are often orbiting around Lagrange points, in particular SEL2, which is about 2 million km from Earth. Thus, the TT&C typically targets a few kbps for both TC and TM, and uses a residual carrier modulation with a moderate coding rate, like those of CC or concatenated. The PDT subsystem instead can target a few tens of Msps while being limited in bandwidth (see Section II-B). Thus, a combination of GMSK $BT = 0.25$ with (possibly) punctured CC or

Table VIII
LIST OF ALLOWABLE TM CHANNEL CODES AT CADU LEVEL.

Code	Rate
CC	1/2
Punctured CC	2/3, 3/4, 5/6, 7/8
LDPC	1/2, 2/3, 4/5, 223/255 ($\sim$7/8)

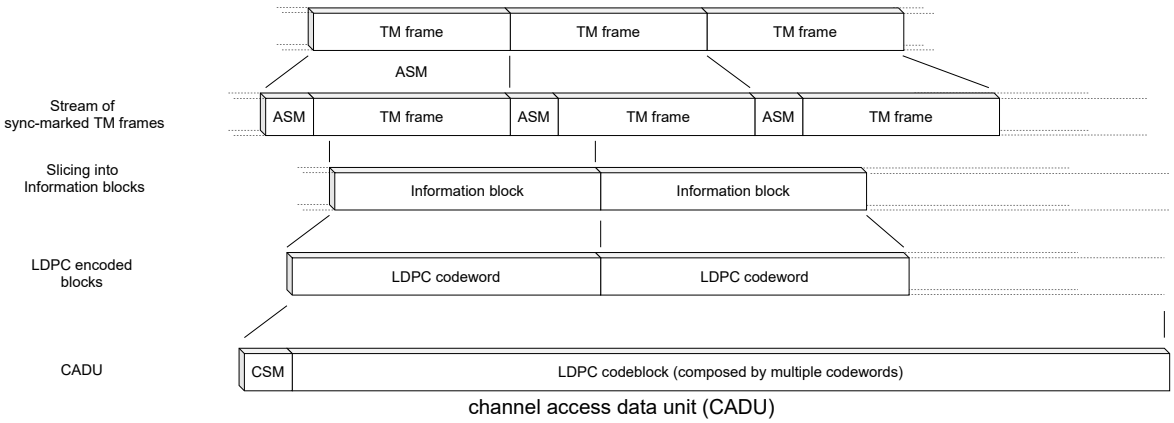

Figure 21. Encapsulation of TM frames into a CADU, when LDPC at CADU level is adopted: a stream of synch-marked TM frames is sliced into information blocks, that are then LDPC encoded. Finally, a multiple number of LDPC codewords are collected into a LDPC codeblock, and attached with the CSM.

Table IX
COMMON DESIGN OF TM LINKS (MODULATION, CODING, AND FREQUENCY ALLOCATION) IN ESA MISSIONS.

Mission type	TT&C	PDT
Earth Observation	SP-L/PM or Filt. OQPSK RS only, or Concat. S-Band	8PSK-TCM RS (for 8PSK-TCM) X-Band
Science (near Earth)	NRZ/BPSK/PM or SP-L/PM CC, Concat. X-Band	GMSK (BT=0.25) Punctured CC, Concat. X-Band
Science (deep space)	NRZ/BPSK/PM Turbo or LDPC X-Band	GMSK (BT=0.5) Turbo or LDPC X-Band

concatenated is often a viable solution;

- Deep space missions are usually power limited. The TT&C cannot support more than a few kbps, and can target symbol rates as low as ∼7.8 sps. Similarly, the PDT symbol rate is usually in the order of some tens of kbps. Consequently, the use of low rate coding is often the best solution. Since the bandwidth is not a concern, deep space missions usually resort to resilient modulations as NRZ/BPSK/PM, GMSK $BT = 0.5$, or unfiltered suppressed carrier modulations.

D. Tracking

So far, the paper mostly dealt with the TC and TM functions. In this section, we will focus on the third fundamental function of the TT&C subsystem: the tracking or, in other words, the measurement of a satellite range and range rate.

To perform range measurements, a dedicated RNG signal is transmitted from the ground station to the spacecraft and then back to Earth (as shown in Figure 1). The distance between the spacecraft and the ground is derived from the round trip light time of the signal. To illustrate the basic concept, let us consider a pure tone signal with frequency f_{T} that is transmitted from the ground station and received back with a phase difference of $\Delta\theta$. An estimation of the spacecraft distance $\hat{r}$ can be obtained as

$$\hat{r} = \frac{1}{2}\frac{\Delta\theta}{2\pi f_{\mathrm{T}}}\mathrm{c}\,,$$

where c is the speed of light. Although this kind of measurement is easy to implement, it has a major flaw: the selection of f_{T} is a trade-off between accuracy and ambiguity. Namely, at high frequency, the tone will complete several 2π cycles in its round trip, causing the measurement to have an ambiguity equal to $\mathrm{c}/f_{\mathrm{T}}$. For instance, if the frequency tone is in the order of 100 kHz, the ambiguity will be in the order of thousand meters, way lower than the hundred/thousand kilometers usually required for orbit determination. On the other hand, at a low frequency of 100 Hz, a small error of, for example, 0.01 rad in the phase estimation, will result in a measure with a poor accuracy of about 2000 meters. To tackle this issue, different solutions can be adopted. A first possibility is to use a multi-tone RNG signal which uses both high and low frequency tones. This was the rationale behind *code ranging*, defined in the ECSS standard [46]. The complex base-band mathematical expression of the code ranging signal reads

$$r(t) = e^{jm_{\mathrm{r}}\Phi(t)}\,, \tag{16}$$

where $\Phi(t)$ is the RNG signal, and m_{r} the modulation index. This signal, in turn, is a sub-carrier with frequency f_{T} (defined as the *fundamental tone*) and phase-modulated as

$$\Phi(t) = \sin\left(2\pi f_{\mathrm{T}}t + m_{\mathrm{T}}C_n(t)\right)\,,$$

where m_{T} is the tone modulation index, and $C_n(t)$ is a 2^n-length code adopted for ambiguity resolution (being n a design parameter). Namely, $C_n(t)$ has expression

$$C_n(t) = \sum_k c_k \mathrm{rect}\left(f_{\mathrm{T}}t - k\right)\,,$$

where $c_k \in \{\pm 1\}$ belong to a 2^n-length periodic sequence obtained as

$$c_k = q_{1,k}\cdot q_{2,k}\cdot q_{2,k}\cdot\cdots\cdot q_{n,k}\,,$$

and $q_{i,k} = (-1)^{\lfloor k/2^{i-1}\rfloor}$.

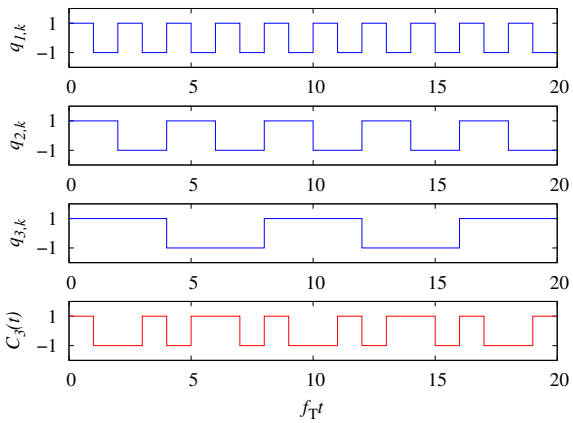

Figure 22. Plot of the $3-$length code, obtained as composition of three tones with frequency $f_T/2$, $f_T/4$, and $f_T/8$.

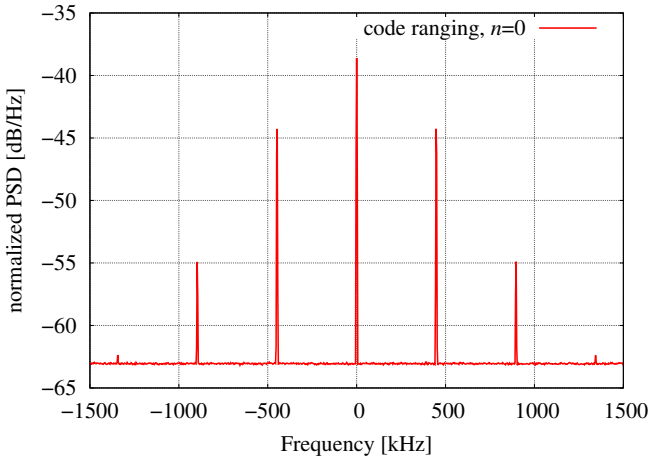

Figure 23. Normalized PSD for a code ranging signal, $n = 0$, frequency tone $f_T = 448$ kHz, and modulation index $m_r = 1.0$ rad/peak.

Although the expression of the code ranging signal can appear quite cumbersome, it is nothing else than a tone of frequency f_T, phase modulated, with the introduction of lower frequencies by means of $C_n(t)$. In particular, if we adopt the Jacobi-Anger approximation (as done in Section III-A), the code ranging signal can be expressed as

$$r(t) \approx \mathrm{J}_0(m_r) + 2j\mathrm{J}_1(m_r)\sin(2\pi f_T t + m_T C_n(t))\,. \quad (17)$$

For $n = 0$, it holds $C_0(t) = 1$, and the signal is nonetheless than a residual carrier with power fraction equal to $\mathrm{J}_0(m_r)^2$, and a tone with power fraction equal to $2\mathrm{J}_1(m_r)^2$. These are complemented by tone replicas at multiples of f_T due to the higher-order terms of the Jacobi-Anger formula. Differently, for $n > 0$, the code $C_n(t)$ introduces lower frequencies down to $f_T/2^n$. Figure 22 shows the example of the 2^3-length $C_3(t)$ (in red) and the analog equivalent of its sub-components $q_{1,k}, q_{2,k}, q_{3,k}$ (in blue). It can be seen that the sub-components represent a square wave with frequency $f_T/2$, $f_T/4$, and $f_T/8$, respectively, while the resulting signal $C_3(t)$ is obtained as a combination of such waves.

The overall effect can be seen in Figure 23 and 24 that show the spectra for (16) with $n = 0$ and $n = 2$, respectively, when the resolution bandwidth is $R_{BW} = 4$ kHz. Both cases have modulation index $m_r = 1.0$ rad/peak, frequency tone $f_T = 448$ kHz, and (for $n = 2$) a tone modulation index m_T equal to $\pi/4$ rad/peak.

Beyond code ranging, there is a second solution that relies upon the same principle: the *pseudo noise ranging* (PN ranging). Namely, it adopts a ranging sequence that combines PN sequences, each characterized by a different period and thus different harmonics. This kind of waveform, standardized by the CCSDS [47], was introduced to cope with high position accuracy requirements of future space missions. For this reason, the standard foresees the possibility of implementing regenerative ranging [48] in low SNR scenarios or when high accuracy is demanded. As for the code ranging, the complex base-band signal can be written in the form reported in (16),

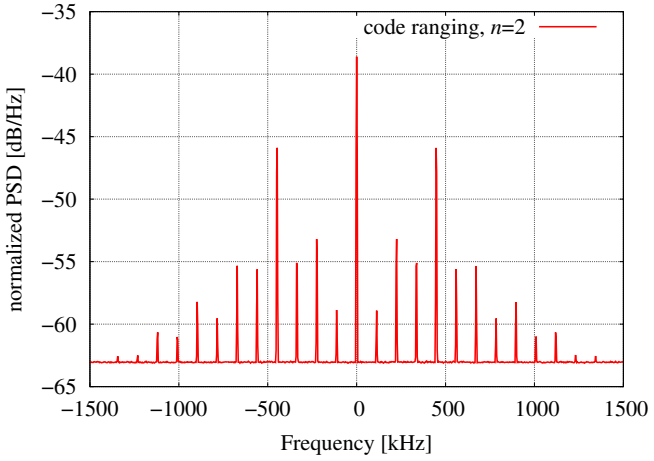

Figure 24. Normalized PSD for a code ranging signal, $n = 2$, frequency tone $f_T = 448$ kHz, modulation index $m_r = 1.0$ rad/peak, and tone modulation index $m_T = \pi/4$ rad/peak.

where $\Phi(t)$ is defined as

$$\Phi(t) = \sum_k c_k h(t - kT_c)\,, \quad (18)$$

being T_c the chip time, and $c_k \in \{\pm 1\}$ the chips belonging to the ranging sequence. Moreover, the chip pulse shape $h(t)$ reads

$$h(t) = \begin{cases} \sin(\pi t/T_c) & t \in [0, T_c] \\ 0 & \text{elsewhere} \end{cases}.$$

The ranging chip sequence $\{c_k\}$ is constructed as a weighted voting expressed as

$$c_k = \mathrm{sign}(\nu C_{1,k} + C_{2,k} - C_{3,k} - C_{4,k} + C_{5,k} - C_{6,k})\,,$$

where $C_{1,k}, ..., C_{6,k}$ are six periodic *component sequences* listed in Table X, where $C_{1,k}$ acts as a "clock". The weighted-voting parameter ν determines the type of resulting sequence, which can be a balanced Tausworthe 4B (T4B) if $\nu = 4$, or 2B (T2B) if $\nu = 2$. The ranging chip sequence can be efficiently generated using a sequential machine (see Figures 2-2 and 2-3

in [48]), composed of six shift registers, one per component, and a combinational circuit that performs that weighted voting.

Once again, the ranging signal expression appears quite cumbersome. However, if we assume for a moment that $c_k \approx C_{1,k}$, we obtain that $\Phi(t) \approx \sin(\pi t/Tc)$. Thus, by using again the Jacobi-Anger identity, we can approximate the PN ranging signal as

$$r(t) \approx \mathrm{J}_0(m_\mathrm{r}) + 2j\mathrm{J}_1(m_\mathrm{r})\sin(\pi t/T_c)\,,$$

that is none other than a residual carrier with a frequency tone in $1/2T_c$. In reality, because of the other components, $\{c_k\}$ deviates from the perfect clock, and other harmonics appear in the ranging signal. It can be shown that the first-order approximation reads [48]

$$r(t) \approx \mathrm{J}_0(m_\mathrm{r}) + 2j\xi\mathrm{J}_1(m_\mathrm{r})\sin(\pi t/T_c)\,,$$

where ξ is a coefficient that takes values in $[0, 1]$: the closer is to 1, the more $\{c_k\}$ tends to be the ideal clock $C_{1,k}$. On the other hand, it can be shown that the acquisition time will be longer [48].

The two sequences T4B and T2B, have $\xi = 0.9387$ and 0.6274, respectively. If we think the clock $C_{1,k}$ as the fundamental frequency tone, we realize that the T4B trades high position accuracy at the expense of a longer acquisition time. Conversely, the T2B can acquire the ranging sequence in a shorter time at the expense of poorer accuracy. Instead, for both PN sequences, the phase ambiguity is resolved by means of the other components $C_{2,k}, ..., C_{6,k}$ that, having a longer period, can be thought as the lower frequency tones.

As an example, Figures 25 and 26 show the normalized PSD for the T4B and T2B signals, respectively, with $m_\mathrm{r} = 0.75$ rad/peak, and a normalized resolution bandwidth of $R_{BW}T_c = 0.03$. As expected, both spectra are characterized by a residual carrier component that has PSD equal to $\mathrm{J}_0(m_\mathrm{r})^2/R_{BW}T_c$ in correspondence of the carrier frequency, and PN components located at odd multiples of the clock frequency $1/2T_c$. Furthermore, we can observe that the T4B clock has a higher power than the T2B clock, as indicated by their power ratio (of the two ξ^2 values in Figures 25 and 26) of approximately 3.5 dB.

The range measurement, whether obtained with code or PN ranging, is complemented with range rate measurements. For this, the ground station estimates the range rate by measuring the Doppler on the TM signal. However, to avoid the spacecraft transponder frequency stability affecting the estimation, typically, the measurement is done in a *coherent mode*. Namely, at TC arrival, the transponder locks on the uplink carrier frequency and performs a turn-around, i.e., generates a TM signal whose carrier frequency is coherent with the uplink one using a multiplicative ratio. The possible values of turn-around ratios depend on the adopted frequency allocations and can be found in the ECSS [11]. For instance, if we consider a space mission having uplink and downlink in S-Band, with an uplink frequency of, for example, 2030 MHz, ECSS foresees a turn-around ratio equal to 221/240. Consequently, the downlink frequency shall be $2030 \cdot 240/221 = 2204.52$ MHz. Further details about the turn-around function will be given in Section IV.

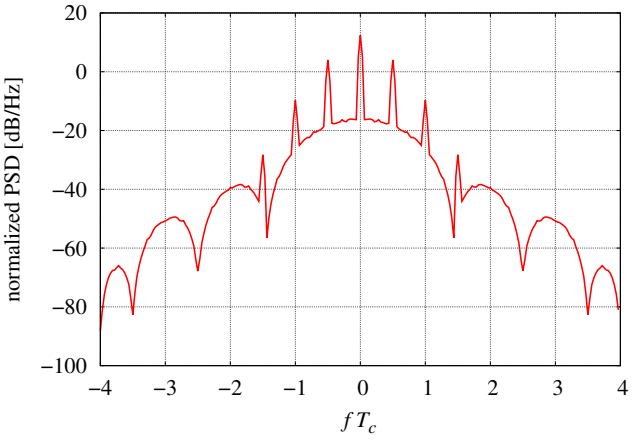

Figure 25. Normalized PSD for T4B PN ranging signal, modulation index $m_\mathrm{r} = 0.75$ rad/peak.

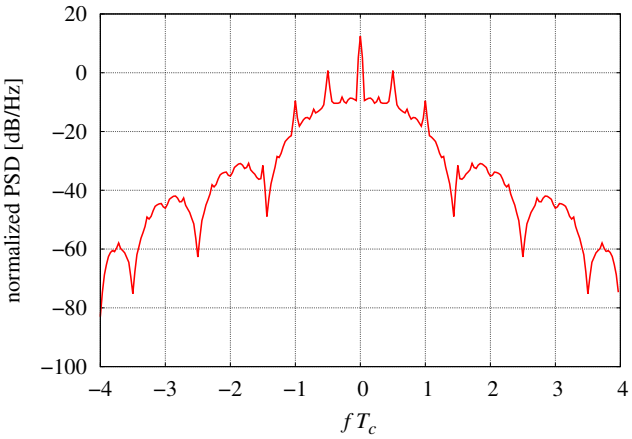

Figure 26. Normalized PSD for T2B PN ranging signal, modulation index $m_\mathrm{r} = 0.75$ rad/peak.

E. Simultaneous communications and tracking

It is standard practice to simultaneously transmit information (telemetry/telecommand) while tracking the satellite. Generally, this is achieved through the combination (in phase) of a phase-modulated ranging signal $r(t)$ and a residual carrier telemetry/telecommand signal $s(t)$. Mathematically,

$$s(t)r(t) = e^{jm_\mathrm{x}x(t)}e^{jm_\mathrm{r}\Phi(t)}\,,$$

where the two exponential functions are the telemetry signal and the ranging signal as defined in (6) and (16), respectively. In the case of an NRZ/BPSK/PM telemetry signal and the code ranging, using the Jacobi-Anger identity and keeping only the first-order terms, we can see the overall signal approximated as

$$\begin{aligned} s(t)r(t) \quad \approx \quad & \mathrm{J}_0(m_\mathrm{x})\mathrm{J}_0(m_\mathrm{r}) + 2j\mathrm{J}_0(m_\mathrm{r})\mathrm{J}_1(m_\mathrm{x})x(t) \\ & +2j\mathrm{J}_0(m_\mathrm{x})\mathrm{J}_1(m_\mathrm{r})\Phi(t)\,. \end{aligned} \tag{19}$$

It can be noticed that the overall residual carrier is $\mathrm{J}_0(m_\mathrm{x})\mathrm{J}_0(m_\mathrm{r})$, while on the quadrature component, both the

Table X
COMPONENTS OF THE PSEUDO-NOISE RANGING SEQUENCE.

Component	Period	Component period chips
$C_{1,k}$	2	+1 −1
$C_{2,k}$	7	+1 +1 +1 −1 −1 +1 −1
$C_{3,k}$	11	+1 +1 +1 −1 −1 −1 +1 −1 +1 +1 −1
$C_{4,k}$	15	+1 +1 +1 +1 −1 −1 −1 +1 −1 −1 +1 +1 −1 +1 −1
$C_{5,k}$	19	+1 +1 +1 +1 −1 +1 −1 +1 −1 −1 −1 −1 +1 +1 −1 +1 +1 −1 −1
$C_{6,k}$	23	+1 +1 +1 +1 +1 −1 +1 −1 +1 +1 −1 −1 +1 +1 −1 −1 +1 −1 +1 −1 −1 −1 −1

telemetry data and the ranging signal can be found. For limiting the mutual interference between the information $x(t)$ and the ranging tones of $\Phi(t)$, typically, the sub-carrier frequency f_{x} and the fundamental tone f_{T} are chosen "far enough" and exploiting the spectral nulls. More details about the selection of these two values can be found in [46].

A similar result can be obtained for a SP-L/PM telemetry signal by substituting in (19) the $\mathrm{J}_0(m_{\mathrm{x}})$ term with $\cos(m_{\mathrm{x}})$ and $\mathrm{J}_1(m_{\mathrm{x}})$ with $\sin(m_{\mathrm{x}})$. Additionally, both the NRZ/BPSK/PM and SP-L/PM can be combined, as an alternative, to a PN ranging signal by properly choosing the PN clock frequency [48].

If, on the one hand, low-rate residual-carrier modulated transmissions are either combined with the code or PN ranging, the standards establish high-rate suppressed-carrier signals (e.g., >1 Msps) to be coupled with PN ranging only by using a GMSK-modulated telemetry signal [49]. Also, in this scenario, the telemetry signal acts as additional noise to the ranging. Vice versa, the latter disrupts the correct reception of the telemetry stream. For this reason, a proper choice of the two modulation indexes (m_{x} and m_{r}) is required for managing the power sharing and the reciprocal interference, and it is strongly recommended to adopt interference cancellation schemes at the receiver (e.g., those provided in [49]).

F. Sizing of the links

In the previous sections, we provided a thorough description of the signals adopted for TC, TM, and RNG. In this section, we focus instead on their sizing for spacecraft missions by using a well known tool in telecommunications engineering: the link budget. The link budget determines the received power by summing up each loss and gain to which the transmitted signal is subject when traveling over the communication channel. The key formula that summarizes the link budget for a spacecraft mission is an instance of the *Frijs transmission equation* [50] that, in dB, reads

$$\left(\frac{P_{\mathrm{RX}}}{N_0}\right) = \mathrm{EIRP} + \left(\frac{G}{T}\right) - L - k_B - \alpha\,, \qquad (20)$$

where, P_{RX}/N_0 is the ratio between received power and noise spectral density, EIRP is the effective isotropic radiated power, L the path loss, k_B is the Boltzmann's constant, G/T is the receiver gain over noise temperature of the receiver antenna, and α includes other impairments/losses that the signal experiences before demodulation (atmospheric, pointing, demodulation, etc.). Although the formula is rather simple, new engineers in the TT&C field can sometimes have difficulties in finding the right values to use and how to lay down a link budget in compliance with the standards. In this respect, this section focuses on the basics specific to the TT&C field.

For instance, the path loss accounts for the attenuation that the electromagnetic signal suffers during propagation from the transmitter to the receiver. Since satellite links move through free space, the path loss is defined, in logarithmic form, as

$$L = 20\log_{10}\left(\frac{4\pi s f}{c}\right)\,,$$

where, f is the carrier frequency of the signal, s the distance, and c the speed of light. The distance s is the satellite *slant range*, i.e., the actual distance from the ground station (a function of the altitude and elevation angle).

The atmospheric loss, another relevant element in the link budget, is a highly variable parameter, strongly dependent on the weather and climatic conditions, hard to predict, and its estimation requires good knowledge of ITU-R models. Luckily, there are free available software tools that can help the TT&C engineer. For instance, CNES developed a dynamic link library to compute the atmospheric losses affecting the Earth-to-space and space-to-Earth transmission links [51].

Similarly, ESA makes available the tracking stations (ESTRACK) facilities manual [13] that reports the characteristics of the ESA ground stations such as the G/T, ground station coordinates (needed for deriving the atmospheric losses), and the adopted station modems, possibly including the demodulation losses.

Traditionally, the link budget for spacecraft missions was computed assuming the worst-case scenario. This approach is inefficient as it assumes the unlikely event in which all the terms involved in the calculation simultaneously take on their worst-case values. To optimize the link budget and thus efficiently design the communication system, space missions usually adopt the procedures in the ECSS standard [11]. According to this, one shall consider as many sets of parameters as the possible scenarios that involve different spacecraft antennas, ground stations, bit rate, etc., and compute a dedicated link budget for each. Focusing on one set, each of those parameters is characterized by its nominal, adverse and favorable values.

The link budget can be computed using a nominal or a statistical approach. The former obtains the design SNR by summing up the nominal values of all the involved parameters. Alternatively, the second approach relies upon a statistical method [52] and is the best way to optimize the communication system design. It treats each parameter involved in the computation as a random variable characterized by a

Table XI
EXAMPLE OF LINK BUDGET WITH NOMINAL, FAVORABLE, AND ADVERSE VALUES.

Parameter	Nominal	Favorable	Adverse
Altitude [km]	700	700	700
Elevation angle [deg]	5	5	5
Slant range s [km]	2563.13	2563.13	2563.13
Frequency f [MHz]	2250	2250	2250
RF output [dBW]	-5	-4	-6
Antenna gain [dBi]	-3	-2.9	-3.1
RFDN loss [dB]	4	3.9	4.1
EIRP [dBW]	-12	-10.8	-13.2
Path loss L [dB]	167.7	167.7	167.7
Atmospheric loss [dB]	0.9	0.9	0.9
G/T [dB/K]	21.4	21.5	21.2

probability density function (pdf). Then, using the central limit theorem, the SNR is approximated by a Gaussian pdf. The ECSS standard [11] encloses a table listing all the probability distributions associated with the link budget parameters. Finally, to account for the uncertainties, both approaches add a margin.

From practical experience, a margin of 3 dB is enough for the nominal link budget. For the statistical approach, [11] defines that the margin based on the *mean* -3σ, and *worst case root-sum-square* (worst case RSS) shall be higher than 0 dB.

In the following, we present a simplified example of a link budget computation for a TM link. Consider the hypothetical scenario of a TT&C transmission from an EO satellite orbiting the Earth at around 700 km above the surface. In this scenario, the minimum ground station elevation angle to the Kiruna ground station, having $G/T = 21.4$ dB/K, is 5 deg. By using geometrical calculations, it is easy to see that the corresponding slant range s is 2563.13 km. For the TT&C, we assume an S-Band subsystem, as in Figure 2, with a frequency of $f = 2050$ MHz. The subsystem has a (nominal) RF output power -5 dBW, antenna gain -3 dB, and RFDN loss 4 dB. As for the modulation and coding, we consider a format with a required E_b/N_0 of 6 dB and a bit rate $R_b = 1024$ kbps.

Given this input, we derive that the EIRP is -12 dBW and that the path loss is $L = 167.7$ dB. Additionally, using a software tool, we can find that the atmospheric loss at Kiruna, for a 99.9% availability and elevation angle of 5 deg, is about 0.9 dB. These values can be found in Table XI. In line with the standards, we also define favorable and adverse values[7] for: RF output, antenna gain, RFDN loss, and G/T. We then associate a pdf as reported in Table XII. We can then compute the mean μ, the variance σ^2, and the adverse variation ΔA^2 (i.e., the square of the difference between the nominal and adverse value), and create a new link budget table as in Table XIII.

In Table XIV, we include the estimated SNR obtained through the link budget calculation based on: design values, mean -3σ, and worst-case RSS. Namely, for computing the SNR for the design values, we apply (20) directly to the column 'Nominal' of Table XI, obtaining $P_{\mathrm{RX}}/N_0 = 69.44$ dBHz . For the mean-3σ, we repeat the same process on the column 'μ' of Table XIII, and decrease it by 3 times its standard deviation, i.e., $69.39 - 3\sqrt{0.1792} = 68.12$ dBHz. Finally, for the worst case RSS, we take the nominal value P_{RX}/N_0 and decrease it by $\sqrt{\Delta A^2}$, i.e., $69.44 - \sqrt{1.06} = 68.41$ dBHz. As a final step, we compute the residual margin for the three methods. The minimum SNR required is given by

$$\left(\frac{P}{N_0}\right)_{\mathrm{req.}} = \frac{E_b}{N_0} + 10\log_{10}(R_b)\,,$$

that in our example is 66.1 dBHz. Thus, we obtain that the three methods give a margin of 3.34, 2.02, and 2.31 dB, respectively, in line with the ECSS requirement.

[7]It is pointed out that, without loss of generality, in this paper the favorable and adverse values are defined as absolute values. In [11], these values are instead defined as variations w.r.t. the nominal values.

Table XII
PROBABILITY DISTRIBUTIONS AND STATISTICAL VALUES.

pdf		μ	σ^2	ΔA^2
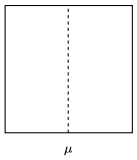	G/T RFDN loss	21.35 4	0.0075 0.0033	0.04 0.01
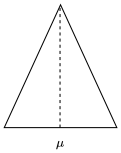	Antenna gain RF output	-3 -5	0.0017 0.1667	0.01 1

Table XIII
EXAMPLE OF STATISTICAL LINK BUDGET WITH THE AVERAGE μ, VARIANCE σ^2, AND ADVERSE VARIATION ΔA^2.

Parameter	μ	σ^2	ΔA^2
Altitude [km]	700	0	0
Elevation angle [deg]	5	0	0
Slant range s [km]	2563.13	0	0
Frequency f [MHz]	2250	0	0
RF output [dBW]	-5	0.1667	1
Antenna gain [dBi]	-3	0.0017	0.01
RFDN loss [dB]	4	0.0033	0.01
EIRP [dBW]	-12	0.1717	1.02
Path loss L [dB]	167.7	0	0
Atmospheric loss [dB]	0.9	0	0
G/T [dB/K]	21.35	0.0075	0.04
P_{RX}/N_0 [dBHz]	69.39	0.1792	1.06

Table XIV
SNR COMPUTATION VIA THE THREE DIFFERENT LINK BUDGET APPROACHES.

Method	P_{RX}/N_0 [dBHz]	Margin [dB]	Required Margin [dB]
Design	69.44	3.34	≥ 3
Mean -3σ	68.12	2.02	≥ 0
Worst case RSS	68.41	2.31	≥ 0

It might seem that increasing the received SNR by enhancing the transmitted power is an efficient way to improve the margins. However, this is not always a viable solution. To limit the risk of interference between communication systems, the ITU regulates the maximum *power flux density* (PFD) whose limits can be found in [11].

The PFD is a measure of the signal strength in the far field, and, assuming free space conditions, it is defined as

$$\mathrm{PFD} = \frac{\mathrm{EIRP}}{4\pi h^2} \max_{\mathcal{F}} \int_{\mathcal{F}-\frac{B_{ref}}{2}}^{\mathcal{F}+\frac{B_{ref}}{2}} S_s(f)\mathrm{d}f\,, \qquad (21)$$

where $S_s(f)$ is the normalized power spectral density of a generic transmitted signal $s(t)$, h is the satellite altitude from the ground, and B_{ref} the reference bandwidth over which the PFD regulations apply. For suppressed carrier modulations, when the channel symbol rate $R_s \gg B_{ref}$, (21) reduces to

$$\mathrm{PFD} \approx \frac{\mathrm{EIRP}}{4\pi h^2} \frac{B_{ref}}{R_s}\,.$$

When residual carrier modulations are adopted, since the majority of the power is devoted to the carrier, (21) becomes

$$\mathrm{PFD} \approx \frac{\mathrm{EIRP}}{4\pi h^2} \alpha_c\,,$$

where α_c is the carrier suppression, that is $\cos(m_{\mathrm{x}})^2$ and $\mathrm{J}_0(m_{\mathrm{x}})^2$ for SP-L/PM and NRZ/BPSK/PM signals, respectively.

It can be noticed that the EIRP adopted in the PFD shall be the highest value experienced during the spacecraft mission. The PFD for the residual carrier modulations is often the most critical and can dictate the maximum transmitted power. In particular, this holds for TT&C systems that use a single RF power for multiple modulation and coding formats.

IV. The Transponder

Having discussed the format of TT&C links, we now have the background knowledge for understanding the basics of a transponder architectural design, the main focus of this section.

As mentioned in Section II, the transponder is the core unit of the TT&C subsystem. It performs the TM transmitting and TC receiving functions while performing the RNG turnaround. To give the reader an idea of such a unit, Figure 27 shows the engineering model of the ESA Solar Orbiter mission [7]. The transponder is usually in the shape of a small box of about 20-25 cm per side, and organized into modules (e.g., one per layer, as shown in the figure) interconnected by means of external coaxial cables. It can have different connectors/interfaces for the RF transmitter output, receiver input, power supply, and monitoring and control.

Although the transponder (as in the picture) is a quite complex unit, typically, its high-level architecture can be summarized as in Figure 28. It is composed by three modules: the RF down and up-conversion modules (to/from intermediate frequency, IF, for receiving and transmitting, respectively), and the digital module. These interface each-other using analog-to-digital and digital-to-analog converters (ADC, DAC). In turn, the transponder digital module interfaces with the spacecraft data-handling subsystem through dedicated electrical lines.

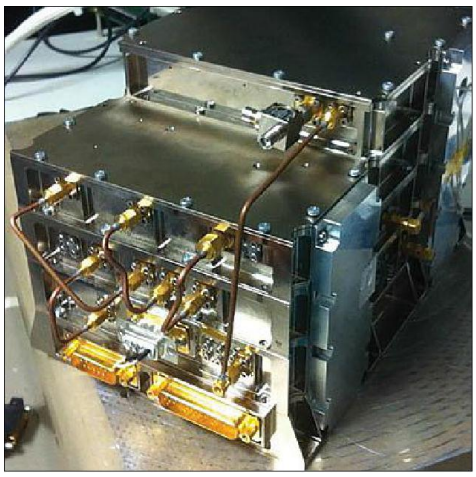

Figure 27. Engineering model of the ESA Solar Orbiter transponder. Image credit [7].

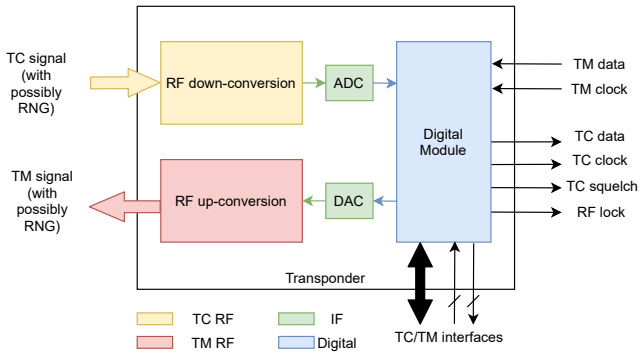

Figure 28. High-level architecture of a transponder unit.

For TC, the transponder provides the data-handling with the demodulated (but usually not decoded) TC data and the TC clock. This information is complemented with a squelch signal (indicating the presence or not of valid TC data) and an RF lock status (specifying if the synchronization chain is locked on the received TC signal). Conversely, for TM, the data-handling provides the stream to be modulated through dedicated TM data and a clock line.

To better understand the functional behavior of the data-handling lines, Figure 29 shows a sketch of the functional behavior of the TC interface. When the transponder receives the TC signal, it takes some time for the receiver synchronization chain to close the loops. This delay is represented in the figure as two symbol times T. After the delay, the transponder declares the lock status on the RF lock electrical line, indicating the synchronization chain is locked on the received TC signal. Then, after an additional delay, the transponder receiver starts to track the TC signal clock and demodulate the TC signal data. Once the TC signal is demodulated, the transponder declares the data validity through the TC squelch.

The transponder executes the monitoring and control function through a dedicated TC/TM interface different from the ones described earlier. Through this interface, the transponder receives internal TC signals from the data handling subsystem

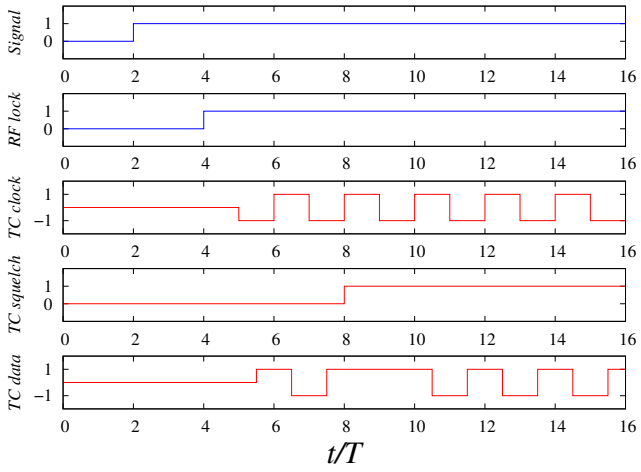

Figure 29. Sketch of the timing diagrams of the transponder TC interface to the data-handling subsystem.

to change its configuration and provides the TM with its current status. The TC/TM interface is often implemented by means of a bi-directional bus and/or dedicated electrical lines. These last are usually preferable for essential TM (e.g., secondary voltage, temperature, etc.) and fundamental TC (usually known as *high priority command*, HPC), that could need to be collected or executed directly, bypassing the bus.

Although not visible in the high-level architecture of Figure 28, the transponder implements an RNG turn-around that (in naïve words) interconnects the receiver and the transmitting chains to form the so-called *RNG channel*[8].

The upcoming sections will explore the functional behavior of the transponder's receiving and transmitting chains in more detail. Specifically, they will focus on the processes of synchronization, demodulation, and RNG turn-around. For clarity, the description will be limited to the case of an NRZ/PSK/PM signal for both TC and TM and the transparent turn-around of a code ranging signal. The case of a filtered suppressed carrier modulation will be provided only for the transmitter. In all cases, it will be assumed that sampling rates are high enough for doing most of the signal processing into the digital core. However, these concepts can be easily extended to all other modulation formats and different digital/analog partitioning. Readers who wish to explore these other scenarios in more detail are encouraged to do so.

A. The receiving chain

The first stage the received signal goes through is the RF down-conversion module. This module can be rather complex, and include multiple stages of mixing, filtering, and amplifications. However, we can summarize its function with the basic block diagram shown in Figure 30. Here, after a first filtering process and a low-noise amplifier (LNA), the received signal frequency is down-converted from RF (f_{RX}) to IF (f_{IF}) through

[8]In case the unit does not have the RNG channel, then it is usually denoted as *transceiver* instead of transponder.

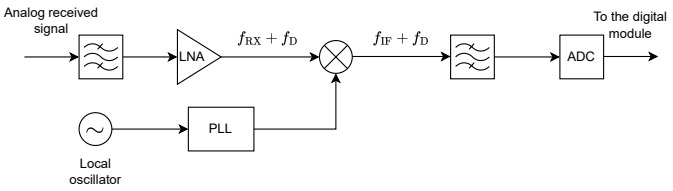

Figure 30. Basic block diagram of the RF down-conversion chain.

a local oscillator and a phase locked loop (PLL) serving as a multiplier. Once the signal is down-converted, the high-frequency components are cut out by a second filter before passing through the ADC. Then, the resultant digital signal reaches the digital module, whose demodulation function is strictly related to the modulation scheme adopted at the transmitting end.

In the case of NRZ/BPSK/PM, the digital module is composed of three main elements. First, a PLL for frequency/phase acquisition[9] and tracking, then a Costas loop which takes care of the sub-carrier tracking and, finally, a data transition tracking loop (DTTL) for recovering the symbol timing.

The block diagram of a PLL is sketched in Figure 31, where the circuit separates the in-phase and quadrature components of the received signal (a phase combination of telemetry and ranging signals) in two different branches. In line with the concepts expressed in Section III-E, when in lock, the upper-most branch carries the in-phase component $\mathrm{J}_0(m_{\mathrm{r}})\mathrm{J}_0(m_{\mathrm{x}})$. The lower carries instead the quadrature component, split (through filtering) in the telemetry and ranging component $2\mathrm{J}_0(m_{\mathrm{r}})\mathrm{J}_1(m_{\mathrm{x}})x(t)$ and $2\mathrm{J}_0(m_{\mathrm{x}})\mathrm{J}_1(m_{\mathrm{r}})\Phi(t)$, respectively. The quadrature branch also acts as a loop error reference for computing the control word (CW) that controls a numerically controlled oscillator (NCO) that generates the local carrier. When the error is 0, i.e., the PLL is locked, the in-phase branch reaches a high value that acts as an indicator for setting the RF lock status. Moreover, whether the transponder is working in a coherent mode, as soon as the error becomes 0, the estimated frequency, scaled by the turn-around ratio (K in the figure), can be adopted by the transmitter.

Recalling the definition of NRZ/BPSK/PM, the data modulates a sub-carrier which requires a tracking algorithm. Due to the presence of data, this can be done using a *Costas loop* [54], whose block diagram is sketched in Figure 32. In naïve words, the Costas loop uses as an error the quadrature component of the sub-carrier multiplied by the data on the in-phase component for adjusting the sign. Hence, if the input of the Costas loop in complex base-band is $a_k e^{j\phi}$ (where a_k are binary symbols, and ϕ the sub-carrier phase error) the loop uses as an error reference $a_k^2 \cos(\phi)\sin(\phi) \approx \phi$, when ϕ is small.

It follows a DTTL for timing synchronization and, consequently, symbol demodulation, as depicted in Figure 33. The first component is an interpolator that aligns the input stream

[9]It is pointed out that the carrier acquisition can be aided by the on-ground carrier sweeping procedure. According to this, the ground station transmits an unmodulated carrier that sweeps in a certain frequency range, for ensuring that enters in the PLL *lock-in range* [53].

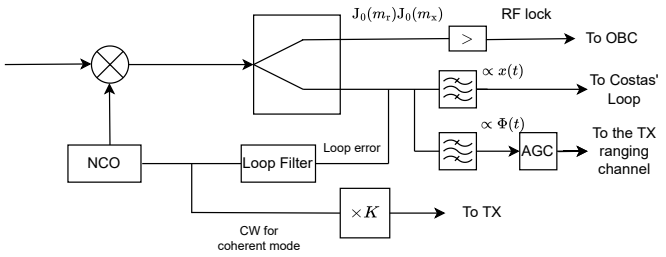

Figure 31. Block diagram of the receiver chain PLL, for the TC carrier frequency/phase tracking.

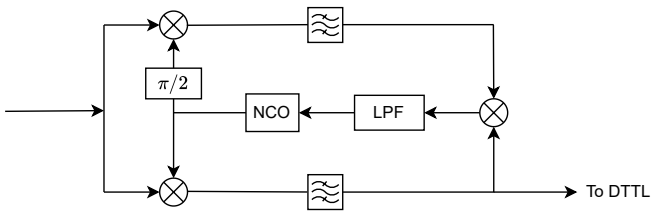

Figure 32. Block diagram of the receiver chain Costas Loop, for the TC sub-carrier tracking.

according to the estimated timing. Its output enters a mid-phase integrator which performs integration between pairs of adjacent bits. For obtaining the loop error, the mid-phase integrator output is then multiplied by the bit-transition, obtained as a difference between the current and the past bit that passed through the in-phase integrator (matched filter). Depending on the sign of the filtered loop error, the interpolator controller, driving the interpolator, will anticipate or delay the estimated symbol time. Finally, as soon as the loop error becomes 0, the data valid status enables the OBC, provided with the data clock, to perform decoding of the data stream coming out of the matched filter.

B. The transmitting chain

Figure 34 shows a possible digital implementation of the residual carrier transmitter with simultaneous transmission of the ranging signal. Starting from the right-hand side, a *coordinate rotation digital computer* (CORDIC, [55]) block generates the NRZ/BPSK signal as provided in (7). Namely, the TM clock, properly scaled, drives the clock of a phase

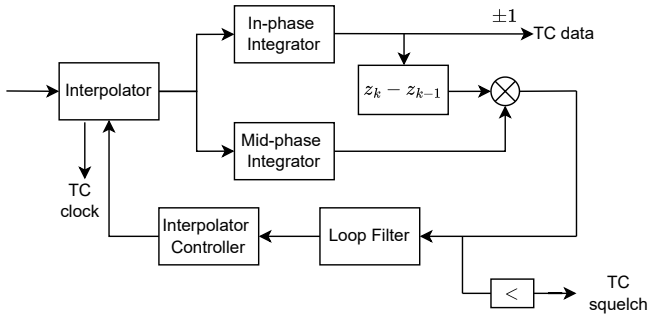

Figure 33. Block diagram of the receiver chain DTTL, for the TC timing synchronization.

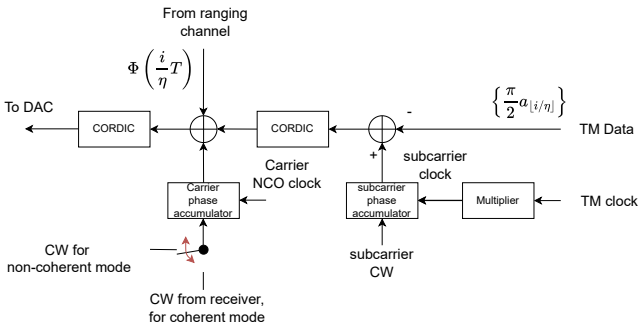

Figure 34. Block diagram for a possible implementation of a residual carrier TM transmitter, with ranging and coherency.

accumulator, whose CW is chosen to generate a sub-carrier phase θ_i with samples

$$\theta_i = 2\pi f_{\rm x}\left(\frac{i}{\eta}\right)T\,,$$

where η is the oversampling factor, and the sub-carrier $f_{\rm x}$ is a multiple of the TM symbol rate (see Table VI). The sub-carrier phase θ_i, together with the (oversampled) TM data scaled by $\pi/2$, provides at the CORDIC output the samples

$$\begin{aligned} x_i &= \cos\left(\theta_i - \frac{\pi}{2}a_{\lfloor i/\eta \rfloor}\right) \\ &= a_{\lfloor i/\eta \rfloor}\sin\left(2\pi f_{\rm x}\left(\frac{i}{\eta}\right)T\right)\,, \end{aligned}$$

which correspond to the samples of $x(t)$ in (7) at instants iT/η.

The NRZ/BPSK samples x_i are fed, together with the ranging samples, to a second CORDIC with a carrier phase value that is controlled by a separate phase accumulator. The resulting signal has samples corresponding to $s(iT/\eta)r(iT/\eta)$, being $s(t)$ and $r(t)$ the target NRZ/BPSK/PM and ranging signals as in (6) and (16), respectively. Namely, the transmitted digital signal has complex base-band expression (w.r.t. the carrier frequency) equal to

$$s_i r_i = e^{jm_{\rm x}x_i + m_{\rm r}\Phi\left(\frac{i}{\eta}T\right)}\,.$$

The carrier phase accumulator can be properly tuned with a fixed CW for generating the target IF when in the non-coherent mode. Differently, for the coherent mode, the CW is provided by the receiver synchronization chain (see Figure 31). In this way, if the Doppler in uplink is equal to $f_{\rm D}$, the transmitted signal becomes

$$s_i r_i e^{j2\pi K f_{\rm D}\left(\frac{i}{\eta}T\right)}\,, \tag{22}$$

where K is the turn-around ratio.

The modulation of a suppressed carrier signal often requires a separate logic into the digital core, especially for those modulation formats that can be implemented with an I/Q modulator. Figure 35 shows a possible digital implementation of a PSK/APSK modulator. The TM binary symbols at its input are up-sampled by a factor η and mapped into PSK/APSK

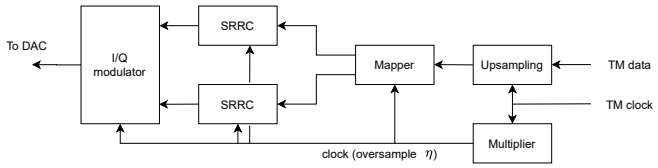

Figure 35. Block diagram of a possible implementation of a suppressed carrier TM transmitter for PSK/APSK signals.

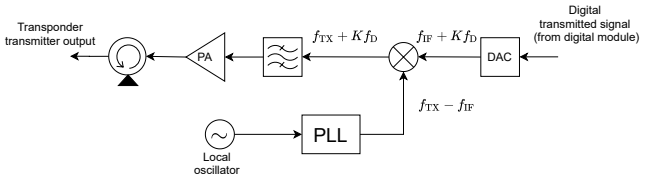

Figure 36. Basic block diagram of the transponder RF up-conversion chain.

channel symbols, thus creating a stream whose I/Q parts (in complex-valued notation) read

$$\sum_k a_k \delta_{i-k\eta} \,,$$

where a_k are the channel symbols belonging to a PSK/APSK constellation, and δ_i is the Kronecker delta. Such a stream is then SRRC filtered and I/Q modulated, thus producing a digital transmitted signal equal to

$$s_i = \sum_k a_k p_{i-k\eta} \,, \tag{23}$$

where p_i are the samples of the SRRC filter at instants iT/η.

For both the residual and suppressed carrier case, the digital transmitted signal in (22) and in (23) goes into a DAC. Its output is fed to the RF up-conversion chain that can be rather complex but whose functions can be summarized with the basic block diagram in Figure 36. The signal from the DAC is up-converted from IF (f_{IF}) to RF (f_{TX}) using a local oscillator and a PLL that provides the target frequencies. In the case of coherency, as shown in the block diagram, the up-conversion to RF is inclusive of the Doppler term Kf_{D}. Finally, the RF signal is fed to a filtering and power amplifier (PA) stage with the possible use of an isolator.

V. Latest Techniques and Open Research Directions

This section provides an overview of some of the most relevant studies, research topics, techniques, and technologies in the field of TT&C. The authors have attempted to summarize the studies and developments that are relevant to future satellite missions while highlighting the main challenges that still need to be addressed. Nevertheless, this section is incomplete: even at the time of writing, many ongoing studies could not be reported here for the lack of space and the sake of clarity. We recommend that readers always check the latest available literature. A good reference is the proceeding of the triennial international workshop on TT&C [56].

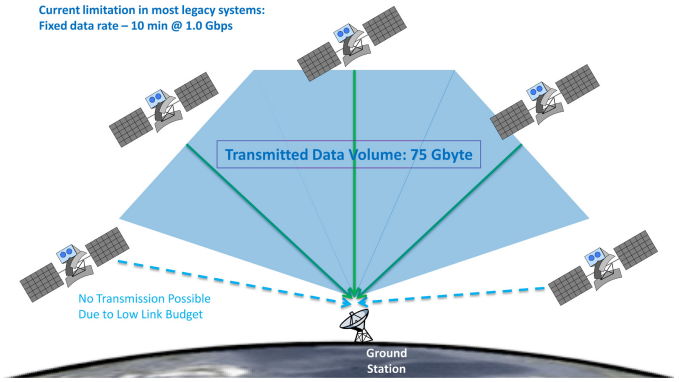

Figure 37. Example of satellite pass with a fixed-rate modcod. Image credit [57].

A. Variable coding and modulation

Most of the ongoing and past satellite missions have a PDT subsystem that implements a single modulation and coding format (modcod) with a fixed bit rate. However, for LEO missions, such an approach has a major drawback: it does not take advantage of the SNR increase along the satellite pass.

To better understand this issue, let us assume a satellite with a PDT link having a fixed-rate QPSK of 1.0 Gbps, 1/2 coding rate (hence 1 GBaud), sized (link budget-wise) for a minimum ground station elevation that provides a pass of about 10 minutes. In Figure 37, the example is represented in cyan. Trivially, the total data volume will be 600 Gbit, i.e., 75 Gbyte. By doing some geometrical calculations, it is easy to show that the ratio between the maximum slant range s, and the minimum one (i.e., the satellite altitude h) is

$$\frac{s}{h} = \frac{1}{h}\sqrt{R_e^2 + (R_e+h)^2 - 2R_e(R_e+h)g(\phi_{\min})} \,, \tag{24}$$

where

$$g(\phi_{\min}) = \sin\left(\phi_{\min} + \sin^{-1}\left(\frac{R_e}{R_e+h}\cos(\phi_{\min})\right)\right) \,,$$

and R_e is the Earth radius. Considering the satellite in the example to have an altitude $h = 700$ km, and $\phi_{\min} = 5$ deg, based on (24), we obtain a ratio of ∼3.6. This translates into an SNR increase during the pass of more than 11 dB (see Section III-F).

Now, imagine taking advantage of this by increasing the bit rate by ∼20% every time that the SNR increases by 1 dB, up to 4 dB and then, decrease the bit rate as the SNR decreases. This will result in a satellite pass like the one in Figure 38, where the satellite transmits, for example, for 1 minute at 1 Gbps, 2 minutes at 1.3 Gbps, 3 minutes at 1.6 Gbps, and (at zenith) 4 minutes at 2 Gbps. This gives a data volume of about 123 Gbyte, with a 64% increase w.r.t. the fixed-rate modcod. This technique is known as *variable coding modulation* (VCM), which consists of nothing else than defining a schedule of modcods along the satellite pass for changing the bit rate as the path loss changes.

While the concept of VCM may seem straightforward, implementing it requires careful consideration of technical details. Specifically, it is important to ensure that changes in bit

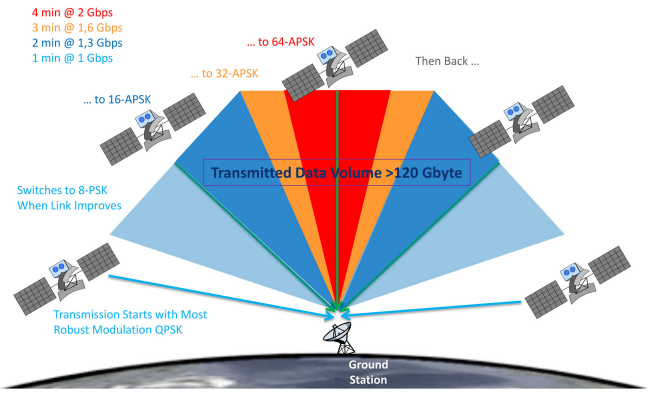

Figure 38. Example of satellite pass with different modcods implementing a VCM strategy. Image credit [57].

rate do not result in link loss or introduce additional overhead or inefficiency, which could compromise the gains achieved through the use of VCM.

To ensure this, a suitable physical layer standard is first required. In this respect, CCSDS defines the VCM standard in [58] for which ESA future missions plan to adopt the instance known as *type 1*, based on serially concatenated convolutional codes (SCCC). The full specification of type 1 - SCCC can be found in [59] (often known in the TT&C community, with abuse of naming, simply as *SCCC standard*). This standard foresees 27 modcods, with PSK/APSK modulations, different coding rates, and efficiency ranging from 0.71 to 5.39 bit per channel symbol. During transmission, the information symbols are organized into a physical layer frame, as shown in Figure 39. The frame starts with a marker of 256 fixed channel symbols for recognizing the beginning. The marker is followed by the frame descriptor, composed of 64 channel symbols encoding (with strong protection) 6 bits that identify the adopted modcod and the optional use of pilots. Both frame marker and descriptor are $\pi/2$-BPSK modulated. It follows the information block that includes 129 600 channel symbols with the selected modcod. Then, the information block can optionally contain blocks of 240 pilots, $\pi/2$-BPSK modulated, every 8100 channel symbols for improving synchronization. This special data structure allows the transmitter to change the modcod at each frame: the receiver simply has to maintain the synchronization based on the frame marker and pilot fields, and identify the modcod adopted in each frame by decoding the descriptor. If we consider the example provided at the beginning of this section, the modcod can be changed every 0.13 milliseconds while having a total overhead of less than 4%.

A second technical aspect is the proper selection of the operational point of the PA in the RF up-conversion chain (see Section IV-B). The choice of operational point requires a trade-off between amplifier nonlinear distortions and transmitted RF power. Considering that different coding rates can address varying levels of nonlinear distortion, each modcod has an optimal output back-off (OBO) [60]. To achieve the best performance, the VCM transmitter has necessarily to change the optimal OBO at the beginning of each frame. This can be achieved by implementing a proper loop between the RF up-conversion chain and the digital board to adjust the power level control. For more information about optimizing the OBO for the SCCC standard, readers can refer to [61].

In conclusion, although no ESA flying spacecraft is currently implementing VCM, this technique is considered a baseline in many EO future missions. Furthermore, it has also been recently proposed for future SRS missions [62].

B. Adaptive coding and modulation and re-transmission protocols

Although VCM is promising, by taking advantage of residual margin that arises from random effects, such as atmospheric losses. As described in Section III-F, the link budget usually allocates a dedicated margin for these effects, that can result in a large inefficiency in specific cases. This is particularly true for LEO missions (mostly EO) with a PDT at high frequency.

To give the reader a better idea, let us consider the EO mission described in Section III-F. In S-Band, the atmospheric loss for an almost complete annual availability (99.9%) at the Kiruna ground station, with 5 deg elevation, is very low and not an issue. However, if we assume a K-Band link instead, the atmospheric loss would increase significantly to around 24 dB, primarily due to rain attenuation. At a lower availability of 95%, the atmospheric loss would be around 7 dB. This means that a significant portion ($24 - 7 = 17$ dB) of the allocated link margin is being used to avoid long outages on approximately 20 “bad days” per year. On the other hand, during the remaining days, the spacecraft link will experience high SNR which will not be fully utilized (especially during sunny days).

Imagine now erasing (part of) this margin, and having a ground station that is able to perform an (almost) real-time SNR estimation for deriving the “link quality”. During the pass, the ground station can then send TCs to switch the bit rate instantaneously based on the link quality. This approach, known as *adaptive coding modulation* (ACM), takes advantage of the best link conditions while implementing VCM.

Looking at the spacecraft communication subsystem architecture, the use of ACM appears almost transparent. It is sufficient that the PDT subsystem implements a VCM standard (as provided in the previous section) and it can change the modcod as soon as the related TC is received. Differently, on the ground segment, things are more complex. Regarding Figure 1, the ACM strategy shall be implemented on the payload TM link: the payload ground station has to measure the link quality, reports it to the MOC that, in turn, will select the modcod and send the TC to the spacecraft by means of the TT&C ground station. It is possible to identify the following major challenges, still open for future research:

- to develop protocols that can efficiently close the loop between payload ground station and MOC;
- to mitigate the ACM performance degradation due to the overall delay from the link quality measurement till the change of the modcode. A possibility is to develop prediction algorithms;

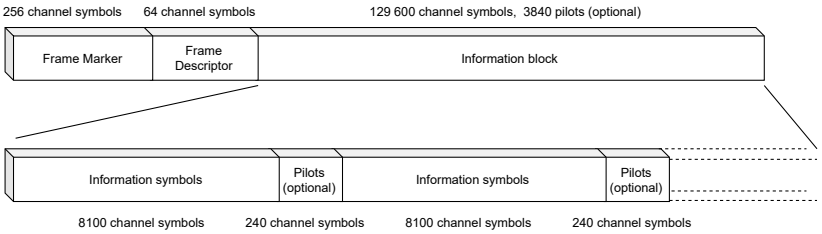

Figure 39. VCM type 1 - SCCC, physical layer frame structure. It is composed by a frame marker (for recognizing the start of frame), a frame descriptor (for identifying the adopted modcod), and an block containing the information channel symbols with (optionally) pilots for aiding the synchronization.

- to overcome the limitations when using two different ground stations. The TT&C and payload ground stations should be as co-located as possible in order to avoid limiting the satellite pass interval during which ACM can be used. Another option, which has not been studied yet, is to develop on-board ACM techniques where the satellite directly measures the link quality and closes the loop on-board

At the time of writing, ESA had already conducted dedicated studies on ACM (e.g., [63], [64]). The agency is currently performing additional research activities to improve the ACM technique and considering it for possible implementation in future EO missions.

As an alternative and intermediate step, ESA is currently considering to adopt a re-transmission protocol known as *CFDP Class 2* that can be seen as ACM implemented at protocol level since it causes a reduction of the net bit rate. Namely, future EO missions using K-Band (like ROSE-L [65]) will have a link budget sizing between 95-99% availability. Instead, the link outages occurred during rainy days will be recovered through data re-transmissions. For further information about CFDP Class 2 functions and performance, the reader can refer to [66]–[68].

C. Simultaneous transmission of high-rate telemetry and PN ranging

As mentioned in Section III-E, for transmitting high-rate telemetry with ranging, standards foresee the simultaneous transmission of PN ranging with high rate GMSK-modulated telemetry [49]. This scheme is highly adopted in SRS missions transmitting in X-Band. On the other hand, for increasing the spectral efficiency, SRS missions (especially near Earth) are considering the adoption of high-order modulations (like those in the SCCC standard [59]) for potentially enabling also the use of VCM [62].

For this reason, the authors in [69] performed a feasibility study on the coupling of PN ranging with high-order PSK/APSK modulations. Namely, it was considered a SRRC-filtered PSK/APSK-modulated telemetry stream reading

$$s(t) = \sum_k a_k p(t - kT)\,,$$

where T is the channel symbol time, $p(t)$ is the SRRC pulse shape, and $\{a_k\}$ are channel symbols belonging to a PSK/APSK modulation. At the transmitter, the telemetry stream and the phase-modulated ranging signals are multiplied (in complex base-band) as

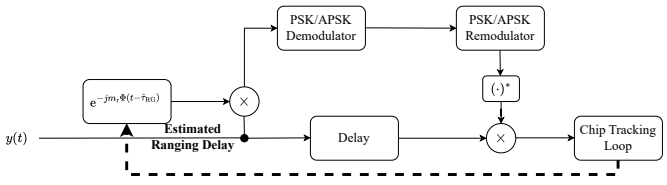

Figure 40. Block diagram of a receiver that allows the simultaneous demodulation of a PSK/APSK modulated signal and tracking of the PN ranging.

$$s(t)e^{jm_r\Phi(t-\tau_{RG})}\,,$$

where $\Phi(t)$ is the PN ranging of (18), and τ_{RG} a generic delay between the two signals.

In the study, it was investigated a receiver scheme that can simultaneously demodulate the telemetry data while tracking the ranging signal. Figure V-C shows the receiver block diagram, where there are two parallel branches in a closed loop: one responsible for demodulating the telemetry signal, while the other for tracking. The upper branch first cancels out the ranging from the received signal by using a locally generated replica and performs demodulation and regeneration of the telemetry signal. Then, the parallel branch performs a complex multiplication for canceling the telemetry signal, and obtaining the ranging signal that inputs the chip tracking loop. The latter tracks the ranging sequence and feeds back the estimated time delay $\hat{\tau}_{RG}$ to the local PN ranging generator.

For this scheme, it was found that the timing jitter has a closed form approximation reading

$$\sigma_\tau^2 \approx T_c^2 \left(\frac{1}{8} \frac{N_0 B_L}{P} + \frac{\sigma_\zeta^2 B_L T_c}{2} \right)\,, \tag{25}$$

where T_c is the chip time, B_L the chip tracking loop bandwidth, P the useful power of the ranging signal, and σ_ζ^2 the normalized sum of the coefficients of the correlation between the ranging and the telemetry signals. It is interesting to notice that while the first term encloses the classical dependency from the SNR in the loop, the second term underlies a floor caused by an additional noise due to the telemetry signal. It can be shown that this noise term is due to the non-constant envelope property of the telemetry stream that, differently from GMSK, cannot be perfectly canceled out from the ranging signal.

The performance results presented in [69] indicate the feasibility of adopting such a communication scheme. In fact, besides the ranging and telemetry reciprocal interference, the BER does not suffer significant degradation, while the ranging timing jitter reveals a floor that, as highlighted by (25), can be decreased by lowering B_L. This behavior is evidenced by Figure 41, which shows the timing jitter, normalized to T_c^2, obtained with a receiver that perfectly demodulates the telemetry symbols. In the figure, the telemetry is a QPSK-modulated signal with a roll-off factor of 0.2, while the ranging modulation index is $m_{\mathrm{r}} = 0.45$ rad/peak. Despite the jitter floor, the tracking capabilities are comparable to the case of adopting the classical GMSK (depicted in blue) when lowering the loop bandwidth.

The study conducted in [69] aimed to determine the feasibility of receiving the combination of spectrally efficient modulations and PN ranging. While it is not optimal for these modulations, the authors deliberately used the same receiver scheme as the one of the GMSK system. Future research could explore the development of a more optimal receiver scheme for this specific application. One possibility involves the use of advanced techniques such as probabilistic graphical models (e.g., factor graphs) and Kalman filtering [70] which showed promising results in improving the accuracy of receiver designs. For instance, factor graphs are a useful tool for visualizing and representing the interaction between the system states. This makes them well-suited for capturing the complex interdependencies between the various variables, and can aid in the efficient performance of Bayesian inference and estimation tasks. Bayesian inference, such as the sum-product algorithm [71], has been used in [72] to approximate the joint posterior of code symbols and phase noise and perform dynamic phase tracking. Similarly, Kalman filtering can be used to estimate the unknown variables of a system and their probability distributions based on noisy observations and can be adapted to work with different types of channel models. For example, in [73], the authors analyze the similarities between the PLL and Kalman filter, emphasizing the advantages of the latter. They provide an example of the application of Kalman filtering in signal tracking for deep space communications, which is characterized by very low SNRs. In this scenario, synchronization poses new challenges that can be more easily overcome with Kalman filtering-based algorithms than with classical PLLs. It is important to mention that these advanced techniques come with their own set of challenges and trade-offs. In fact, they may require more computational resources and can be more difficult to implement. Nonetheless, they show great potential for enhancing the performance of a receiver coupling spectrally efficient modulations with PN ranging.

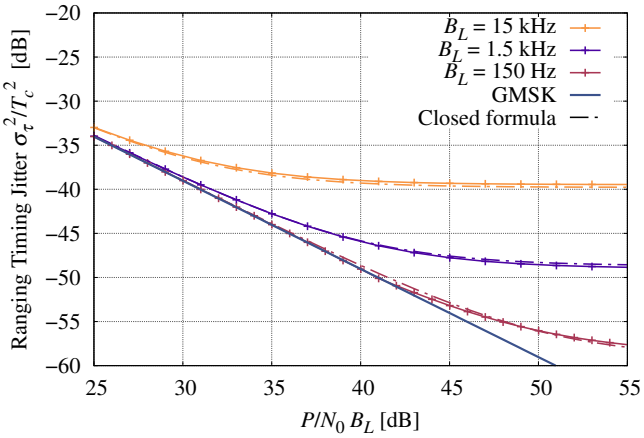

Figure 41. Ranging timing jitter for QPSK, SRRC having roll off 0.2, with PN ranging, $m_{\mathrm{r}} = 0.45$ rad/peak, for different values of the loop bandwidth B_L.

D. TC LDPC codes

The use of BCH(63,56) for TC links is well suited for short and low-rate (i.e., few kbps) communications, especially for links that transmit the required commands a few times a day. However, the BCH has a limited coding gain and, considering the ever-increasing need of higher bit rates, it can sometimes become a major design driver. For instance, a spacecraft could require an additional (and more directive) antenna (just for TC communications) in addition to the two classical LGAs (see Section II). For this reason, the CCSDS defined two LDPC codes having a higher coding gain than the one provided by the BCH code. Since 2021, these two codes are also part of ECSS [35].

The two LDPC codes, usually denoted as LDPC(128,64) and LDPC(512,256), are systematic with a rate of 1/2 and encode 64 and 256 bits into 128 and 512 bits, respectively. For having a good balance between encoding/decoding complexity, coding gain, and coding rate, these codes were designed with a circular structure (more details can be found in [40]). Figure 42 shows the bit error rate (BER) for the two LDPC codes as a function of the energy-per-bit over noise spectral density E_b/N_0 for a BPSK signal. For comparison, the BER of the uncoded and BCH-coded (SEC and TED) BPSK are also included. It can be seen that LDPC can provide an additional coding gain of 3-5 dB w.r.t. BCH, thus making them particularly attractive for future missions. On the other hand, the transponder shall be able to acquire and track a signal at lower SNR, a task that classical algorithms (previously described in Section IV-A) can fail. In this respect, using advanced synchronization techniques (like Kalman filtering/smoothing [73] or Tikhonov algorithm [74]) in a transponder could provide better performance and fully exploit the coding gain. For an overview of the synchronization challenges with LDPC and the open research directions, the reader can refer to [54].

To make the LDPC compatible with the PLOP-2, the CLTU structure, as described in Section III-B (and shown in Figure 15), shall be modified. In particular, the start sequence is modified with a 64-bit pattern, while the tail sequence is a 128-bit pattern that can be optionally used for LDPC(128,64), while it shall be never used for LDPC(512,256). This change takes into account the error correction and detection capability of the two LDPC codes. It allows the user to decide either to have the tail sequence for detecting the end of a CLTU (as for the BCH) or to have the LDPC decoder to fail decoding

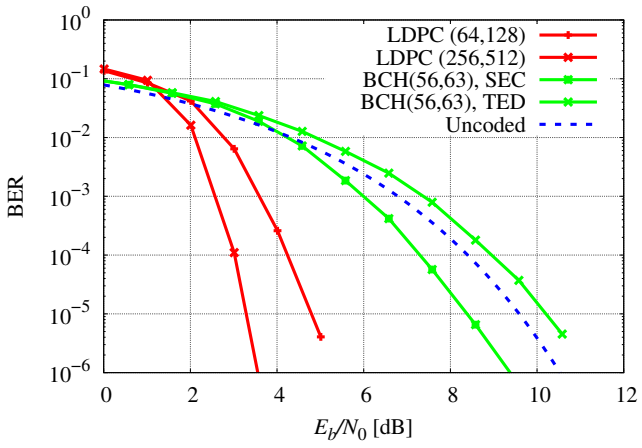

Figure 42. BER curves for a BPSK signal that is coded with LDPC(64,128), LDPC(256,512), BCH(56,63), or BPSK uncoded.

Table XV
TONES NUMBER AND (APPROXIMITED) FREQUENCIES TO BE ADOPTED FOR DDOR.

Allocation	I	$f_{\mathrm{T},i}$
S-Band	1	∼1 MHz or ∼4 MHz
X-Band (deep Space)	2	∼1 MHz or ∼4 MHz, and ∼20 MHz
Ka-Band	3	∼1 MHz or ∼4 MHz, ∼20 MHz, ∼76 MHz

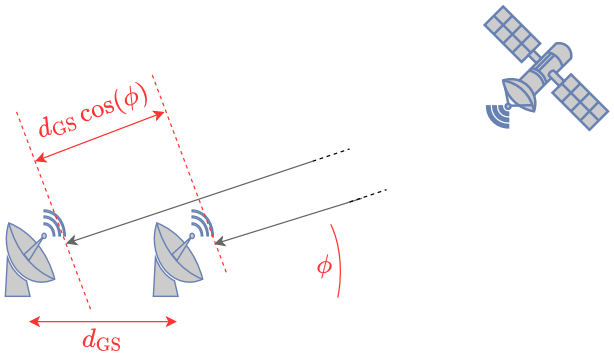

Figure 43. Sketch illustrating the basics of DDOR: the signal sent from the spacecraft is received simulatenously from two ground stations, for estimating the elevation ϕ.

when it over-runs the CLTU. For further information about the design choices for the two LDPCs and the summary of performance, the reader can refer to [40].

E. Delta differential one-way ranging

As described in Section III-D, the TT&C subsystem has a tracking function that allows to obtain the range and range rate measurements. However, these two measurements are insufficient for determining the spacecraft's orbit; the missing coordinates are estimated by taking into account the ground station's motion as the Earth rotates. This approach can achieve an overall accuracy in the order of a few meters and millimeters/seconds, which is usually more than sufficient for a wide range of missions. On the other hand, for scientific missions that involve critical maneuvers, such as gravity assist sling-shots and orbit insertions [1], or radio-science measurements [75], this accuracy may be inadequate.

The *delta differential one-way ranging* (DDOR) is a technique that increases the tracking accuracy [76]. Basically, the DDOR measurement is carried out by transmitting a dedicated signal to two ground stations, and computing the differential delay. For a better understanding of the concept, let us assume a spacecraft that transmits a pure tone signal with frequency f_{T} that is received simultaneously by two ground stations as in Figure 43. If the spacecraft is in deep space, the signal path differential between the two ground stations will be approximately $d_{\mathrm{GS}}\cos(\phi)$, being d_{GS} the distance between the stations, and ϕ their elevation to the spacecraft. Now, if we measure the phase difference $\Delta\theta$ of the signal as received by the two stations, we can estimate the elevation angle as

$$\hat{\phi} = \cos^{-1}\left(\frac{\Delta\theta}{2\pi f_{\mathrm{T}}}\frac{\mathrm{c}}{d_{\mathrm{GS}}}\right), \tag{26}$$

thus obtaining an additional measurement for the orbit determination. In practice, the DDOR relies on a more complicated mathematical framework: Equation (26) shall be extended to three dimensions, and the DDOR signal comprises multiple tones. On the other hand, the underlying concept stays the same.

The DDOR waveform, as defined in the CCSDS standard [32] (recommendation 2.5.6B), is a phase modulation as in (16), where the phase $\Phi(t)$ is

$$\Phi(t) = \sum_{i=1}^{I} \sin(2\pi f_{\mathrm{T},i} t)\,, \tag{27}$$

being I the number of tones, and $f_{\mathrm{T},i}$ the frequency of the i-th tone, to be chosen as provided in Table XV depending on the carrier frequency allocation.

Although the concept appears quite simple, the DDOR measurement is a complex operation. The differential phase is affected by several factors: spacecraft thermal noise, ground station oscillator stability, atmosphere, solar plasma, etc. To mitigate the jitter caused by these factors, the ground stations adopt a quasar for performing a calibration, as sketched in Figure 44. Quasar catalogs are sufficiently dense with sources in S-, X-, and Ka-Band allocations for deep space links and with a position known in the order of nrad. Thus, the ground stations use as a reference a quasar in the same frequency of the transmitted signal, and usually within 0.15 nrad from the spacecraft, so that quasar's and spacecraft's signal path and effects through Earth's atmosphere are similar.

At the time of writing, the DDOR has been adopted in major ESA deep space missions, like *Rosetta*, showing very good performance. However, CCSDS is currently working on an improved version: the *wide-band DDOR* (also known as PN DDOR, [77]). In particular, one of the major impairment in the DDOR measurement is the instrumental phase dispersion, caused by the spectral difference between the quasar (a broadband signal) and the spacecraft signal (composed by pure tones). For reducing the spectral difference, the spacecraft can

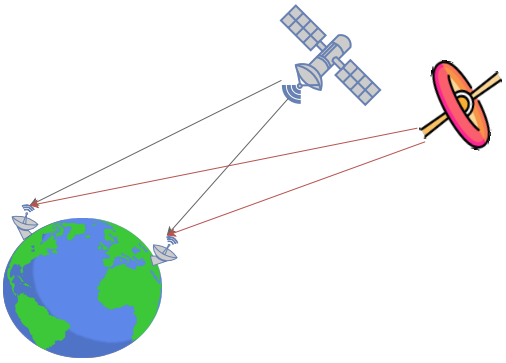

Figure 44. Sketch of the DDOR technique: a reference quasar (in red) is adopted for the calibration of the two ground stations. Subsequently, the two ground stations receive simultaneously the DDOR signal from the spacecraft for performing the measurement.

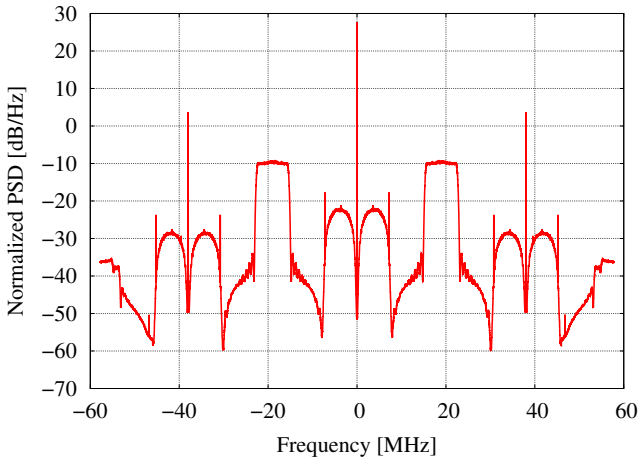

Figure 45. Wide-band DDOR spectrum with modulation index 0.5 rad/peak, roll-off factor 0.1, and chip rate 7.2 Mcps.

modulate a wide-band DDOR signal, with a PN sequence on a sub-carrier as

$$\Phi(t) = \left(\sum_k c_k h(t - kT_c) \right) \sin(2\pi f_{\mathrm{T}} t) \,,$$

being c_k the sequence of chips, T_c the chip time, and $h(t)$ a SRRC shaping pulse. While the standard for chip definition, chip rate, and SRRC roll-off is still under definition, it is generally recommended to select these parameters to match the quasar signal as closely as possible, while still being feasible for hardware implementation. Usually, this is accomplished by resorting to small roll-off factors (e.g., 0.1) and chip rate in the order of several Mcps. For instance, Figure V-E shows an example of a spectrum for a signal filtered with roll-off factor of 0.1, modulation index of 0.5 rad/peak, and a chip rate of about 7.2 Mcps. As it can be seen, the modulated sub-carrier provides a lobe rather flat, thus resembling the quasar.

F. IoT for Earth Observation

EO satellites typically perform planned ground station passes to downlink telemetry one or two times per orbit, while

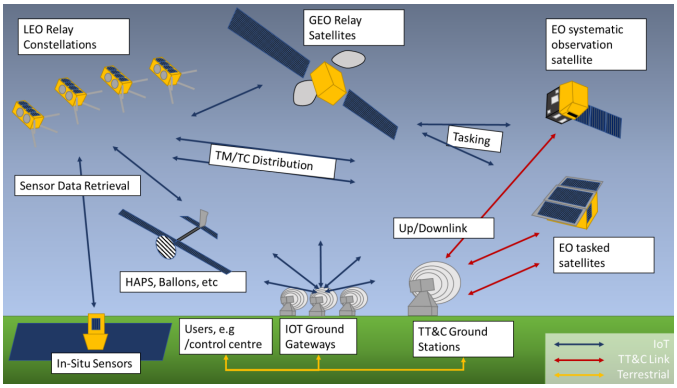

Figure 46. Sketch of IoT for Earth oservation: EO satellites (right-hand side) are beyond the classical TT&C links (in red) have low-rate and low-latency IoT links with in-situ sensors or gateways (in blue), either directly or by means of satellite relay. Image Credit [78].

the upload of telecommands usually occurs only once a day. While this approach works well for systematic observations, such as topography measurements, it is insufficient for urgent tasks required during events like environmental disasters or search and rescue missions. The concept of applying the Internet of Things (IoT) to EO has been recently proposed [78]. Figure 46 illustrates this idea where EO satellites are connected to IoT in-situ sensors or gateways, either directly or via satellite relay, in addition to the classical TT&C and PDT links. The IoT network is designed with a large number of nodes to ensure nearly seamless connectivity. Unlike traditional networks, the links in the IoT-based approach prioritize reducing latency over increasing the data rate

To give an example on how the system can work, imagine an emergency situation (e.g., an environmental disaster) where an EO satellite is required to perform an image acquisition of a specific location. The MOC (see Figure 47) can send the TC for the image acquisition to a ground IoT node that, in turn, can transmit the command (directly or by relay) to the EO satellite closest to the target location. As soon as the TC is received, the EO satellite can perform the image acquisition and provide a thumbnail to the MOC through the IoT nodes. These operations can be potentially carried out in less than one minute. Then, during the next ground station pass (1.5 hour later in the worst case), the satellite can download the full high-resolution picture.

At time of writing, agencies as ESA, NASA, EMSA, EUMETSAT, along with the space industry, are currently defining the first concepts for the use of IoT in EO [80], identifying EO use cases, requirements, market survey, etc. On the other hand, being the concept totally new, several aspects (system architecture, concept of operations, integrity and confidentiality of the links, protocol stack, etc.) still need to be defined and require additional research. In this respect, even if not specific for EO, a good tutorial on the open challenges in satellite IoT can be found in [81].

G. TT&C for mega-constellations

Mega-constellations have emerged as an appealing solution to reduce terrestrial network traffic, provide connec-

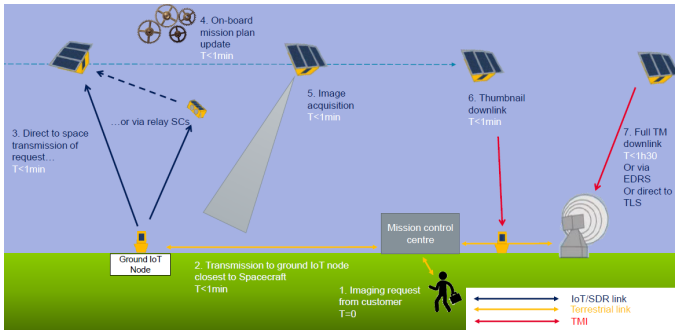

Figure 47. Sketch illustrating an example of a EO satellite performing an image acquisition with a latency of less than one minute, thanks to the IoT network. Image Credit [79].

tivity in remote areas, and enable low-latency communications. Two examples of mega-constellations are Starlink [82] and OneWeb [83], with thousands and hundreds of non-geostationary satellites deployed in LEO, respectively. However, the TT&C for these constellations presents unique challenges, distinct from those of missions targeting EO, space research, and space operations. Unlike these institutional space missions, most of the TC traffic of mega-constellations is utilized to provide services and control the network, requiring much higher data budgets, bandwidths, and data rates. The Earth stations, known as gateways, are distributed globally and feature antenna sizes ranging from 1.5 to 3.5 meters [84], significantly smaller than the conventional 13 or 30-meter antennas used by institutional space missions. Since a single gateway typically serves several satellites (up to four in Starlink [85]), the minimum elevation angle is higher than the classical 5 deg. For example, Starlink gateways employ phased array antennas that achieve a beam pointing accuracy of ± 0.1 deg at any angle from nadir to 40.62 deg [86]. Gateway passes are the result of a trade-off among several variables, including inter-satellite interference, PFD limitations (both on the ground and for GEO satellites), pointing accuracy, and the use of non-directive antennas on Earth [87]. As a result, the visibility time per pass and per day is reduced, posing a greater challenge given the higher data rates involved. Additionally, TT&C for mega-constellations has strict latency requirements similar to those described in the previous section for EO. One possible solution to address this problem is the use of inter-satellite links (ISLs) to accelerate data transmission to Earth and decrease the burden on the ground infrastructure, as already implemented in Starlink [86]. Managing frequency and spectrum allocation can also be a demanding and costly process with a large number of satellites involved. Moreover, maintaining multiple satellites in orbit can be a complex task, especially if the satellites are operated by different entities [88]. In summary, addressing the challenges of TT&C for mega-constellations requires a multi-faceted approach that includes advanced technical solutions and proper network optimization.

H. Survey of additional techniques & other open research directions

In addition to the methods presented in this article, there are several ongoing studies on TT&C and PDT that we cannot describe in-depth due to space limitations. Therefore, the purpose of this section is to offer a brief overview of these studies along with relevant references that readers can consult for more comprehensive information.

Firstly, we will discuss the *telemetry ranging* technique. In naïve words, telemetry ranging is a modulation method that makes the ranging delay measurement completely digital. The spacecraft, instead of transmitting in downlink a replica of the received ranging signal (see Section III-D), samples its code phase and encodes it into 40 bits of the TM transfer frame. This technique has been initially proposed and implemented as a prototype by NASA in the studies [89]–[91]. Currently, ESA is performing internal studies on whether to consider it or not for implementation. Meanwhile, CCSDS has instead published a general recommendation (2.4.24 in [32]) that agencies can adopt as a reference. In this framework, a major open point is to define a detailed definition of the telemetry ranging data link layer that can be (possibly) compatible with the current TM transfer frames and coding standards.

As a second novelty, we mention the *exploitation of the X-Band EESS allocation* for EO missions. As summarized in Table III, such missions usually have a TT&C subsystem in S-Band, and a dedicated X- or K-Band PDT subsystem. However, the ever-increasing number of satellites are making the S-Band congested, causing a complex frequency coordination between the different space agencies and administrations. In light of this, in 2015, the ITU agreed a new frequency allocation in X-Band uplink, in addition to the existing S-Band. This allows TT&C engineers to design an *integrated TT&C and high-rate PDT transponder* that couples the functions of the two subsystems. Thus, the next step is to perform the proper technology development for such architectures. In this respect, ESA funded two studies to implement a breadboard of such a transponder [92], [93].

On a similar topic, we report the *exploitation of the K-Band allocation* for high-rate links. As discussed so far, spacecraft usually have an uplink just meant for TC. However, with the increasing interest in human and robotic exploration around the Moon, future space missions plan to have high-rate telemetry-like links also Earth-to-space (e.g., for connecting an human outpost to Earth). In this respect, entities such as CCSDS and SFCG are paving the way for standardizing such links in the K-Band allocation 22.55-23.15 GHz. Instead, space agencies are performing activities for developing high-rate K-Band spacecraft receivers and ground station transmitters like the ESA ones in [94], [95].

As a final topic of particular interest, we report the *multiple spacecraft per antenna aperture* (MSPA) [96]. Currently, ground stations can only serve one spacecraft at a time. However, for planetary missions (like Martian ones), the ground station beamwidth is able to cover multiple orbiters and landed assets. Thus, instead of having dedicated one-to-one communications for each spacecraft, the ground station could send

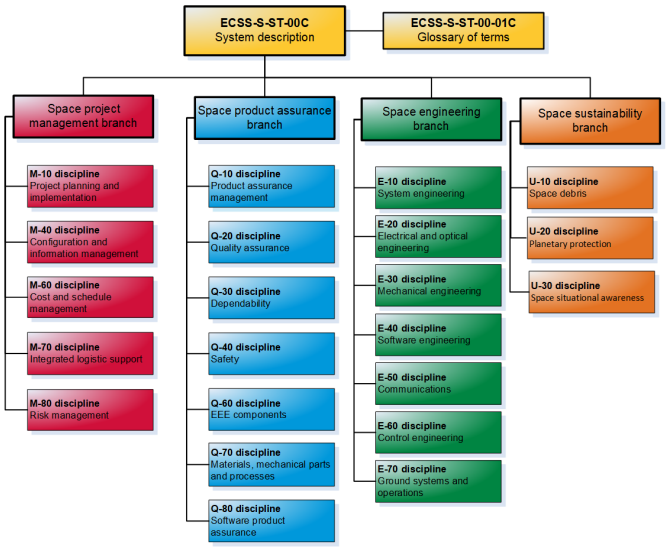

Figure 48. ECSS standards organizational structure, as per 15 September 2021. Image Credit www.ecss.nl.

TC and receive TM simultaneously from multiple spacecraft. To do this, the use of a special code division multiplexing and multiple access scheme has been selected. The way forward is to perform the development of this technology in future transponders and ground stations transceivers [97], [98].

VI. Standardization

Throughout this paper, we often referred to applicable standards as ECSS, CCSDS, and SFCG. These standards are sometimes "intertwined", creating a complex framework that even well-experienced TT&C engineers can sometimes have difficulties understanding it.

The objective of this section is to explain the basics of the organization of space communications standardization and provide the reader with a summary of the applicability of these standards for the design of TT&C subsystems. In particular, a short overview of ECSS and its standard organizational structure will be given in Section VI-A, while Section VI-B and VI-C will provide a brief description of CCSDS and SFCG, respectively, trying to highlight how their standards shall be adopted as a complement to the ECSS.

A. ECSS

The European cooperation for space standardization (ECSS) is an initiative established to develop a coherent single set of standards for use in all European space activities. ECSS includes as members major European agencies such as ESA, CNES, DLR, ASI, UKSA, and a European industry representation.

Figure 48 shows the ECSS organizational structure of the active standards. They are organized into four main branches: space project management, product assurance, engineering, and sustainability, identified by the letter M, Q, E, and U, respectively. On top of these, there is the system (S) branch. In turn, all the four branches are divided into disciplines identified with a serial number ranging from 10 to 80.

For TT&C, the main discipline is *E-50, communications*, and thus all relevant standards have an identification in the format ECSS-E-x-50-n, where x is the kind of document, and n is a number identifying the standard, followed by a letter indicating the revision. At the time of writing, the E-50 includes 17 standards. Limiting to those dealing with the topics of this paper, we can limit the discussion to the standards in Table XVI. The list includes:

- a general *Communications* standard covering definitions, subsystem requirements, and activities to be performed for the design, implementation, and validation of space communication subsystems;
- *ranging and Doppler tracking*, providing details about the code ranging described in Section III-D, and requirements to ensure no impact on the tracking performance;
- the standards for TC and TM modulations and coding formats (as summarized in Section III-B and III-C, respectively), including frequency allocations (as reported in Section II-B), spectrum management and spectral requirements (for compliance with ITU/RR and meeting specific performance), and impairments limitations (e.g., maximum phase noise and minimum carrier suppression).

ECSS often provides a sufficient set of requirements for the design of TT&C subsystems, capturing and properly tracing the outcomes from other standardization groups, or directly applying their standards (e.g., see two CCSDS *Adoption Notice* shown in Table XVI). In many cases, ECSS E-50 can serve as a reliable starting point for TT&C engineers. However, there are some topics that are not always covered by the ECSS requirements, such as advanced TT&C techniques and novel formats. In these cases, referring to other standardization groups is necessary. In addition, ECSS sometimes performs some tailoring of the applicable standards. Some of these exceptions are reported in the following sections.

B. CCSDS

The consultative committee for space data systems (CCSDS) is an inter-agency standardization group that develops standards for data-systems and information-systems to promote interoperability and cross-support among cooperating space agencies. At the time of writing, it is composed of 11 member agencies (including space agencies such as ESA, NASA, JAXA, and ROSCOMOS), 32 observer agencies, and over 119 industrial associates.

Standards are organized in *blue books*, and supported by informative reports, known as *green books*, that contain descriptive material, analysis, test results, etc. On top of these, there are also experimental standards, denoted as *orange books*.

In line with the content of this paper, the main blue books of reference are the *Radio Frequency and Modulation Systems* [32], *TC synchronization and channel coding* [38], and *TM synchronization and channel coding* [44]. The reading of these standards is complemented by the following green books: *Bandwidth-Efficient Modulations* [33], which reviews

Table XVI
SUMMARY OF THE RELEVANT ECSS E-50 STANDARDS THAT DEALS WITH THE TT&C TOPICS DISCUSSED IN THIS PAPER.

Identification	Title	Description
ECSS-E-ST-50, [41]	Communications	high-level standard that includes: • definitions, • communication system requirements (e.g., redundancy, command priorities, etc.), • activities to be performed for the design, implementation, and validation.
ECSS-E-ST-50-02C, [46]	Ranging and Doppler tracking	standard that defines the code ranging (see Section III-D) and requirements about transponder coherency, turn-around, group delay, etc., that directly impact the tracking performance.
ECSS-E-ST-50-05C, [11]	Radio frequency and modulation	standard that defines: • the modulations for TC and TM (Sections III-A, III-B, III-C), • spectrum management and spectral requirements, • impairments limitation.
ECSS-E-AS-50-21C, [45]	Adoption notice of CCSDS TM synchronization and channel coding	document that makes applicable the CCSDS standard for TM synchronization and channel coding (as described in Section III-C), but with specific tailoring for ECSS.
ECSS-E-ST-50-24C, [39]	Adoption notice of CCSDS TC synchronization and channel coding	document that makes applicable the CCSDS standard for TC synchronization and channel coding (as described in Section III-B), but with specific tailoring for ECSS.

filtered PSK and GMSK, along with details on their implementation, and *TC/TM synchronization and coding*, which provides a summary of the concepts and rationales [40], [99].

Since many ECSS agencies are CCSDS members, the standards for TT&C are usually well aligned to the corresponding ECSS ones. However, we report here some major differences:

- *TC modulation, coding, and synchronization*: according to CCSDS, the BPSK modulation can be considered as a modulation format on top of those reported in Section III-B. Additionally, the TC encapsulation can include multiple TC frames per CLTU. Finally, both ECSS and CCSDS allow either the use of BCH or LDPC coding. However, ECSS allows BCH for single error detection only, while CCSDS foresees BCH also for triple error detection.
- *TM coding and synchronization*: CCSDS considers the RS code having a rate of 239/255 (see Section III-C) as a general coding option, while ECSS allows the RS 239/255 only when the TM signal is 8PSK-TCM;
- *Tracking*: code ranging is not a CCSDS standard, while PN ranging is a standard that is exclusive to CCSDS. For PN ranging, CCSDS foresees the blue book [47], complemented by the recommendation 2.5.5A in [32]. The related green book is instead [48]. Then, CCSDS allows the simultaneous transmission of PN ranging with GMSK, as reported in [32], recommendations 2.4.22A and 2.4.22B;
- Finally, also the following standards are part of CCSDS and not of ECSS: DDOR (recommendations 2.5.6B in [32]), VCM (blue books [58], [59], [100] and green books [61], [101]) and telemetry ranging (recommendation 2.4.24 in [32]).

It is worth noting that CCSDS currently has two experimental definitions for extending VCM up to 256APSK, as described in the orange books [102], [103] (experimental standards). In addition, CCSDS is planning to develop dedicated recommendations for K-Band uplink and WB-DDOR, as outlined in Section V.

C. SFCG & ITU

The space frequency coordination group (SFCG) was established to provide a less formal and more flexible environment, compared to the official organs of the ITU, for solving frequency management problems encountered by member space agencies. In naïve words, the SFCG focuses solely on managing frequency allocations for space systems, trying to cover and complement ITU regulations while facilitating consensus among member space agencies on the assignment of specific frequencies and related technical issues.

The main output of SFCG are *technical resolutions* and *recommendations* [15]. These are usually short documents that provide requirements or best practices for designing TT&C subsystems and units. The only difference between resolutions and recommendations is their applicability to projects done by member space agencies and other external bodies (e.g., commercial satellites). Despite this distinction, given the challenges in spectrum management, including recent issues related to 5G interference risks with EO satellites [104], the authors believe that a good TT&C engineer should consider both resolutions and recommendations as mandatory requirements.

It is finally pointed out that SFCG recommendations are often already included as dedicated requirements in the ECSS standard in [11], thus making ECSS is a good starting point. However, since ECSS may not always be up-to-date, particularly with regard to future Lunar and Martian missions, it is recommended that the reader also consult the SFCG website for the latest resolutions and recommendations.

VII. FAMOUS CASES OF TT&C ISSUES AND LESSON LEARNED

In conclusion, we present two well-known examples of space missions that encountered major TT&C issues, namely *Beagle-2* and *Cassini-Huygens*, and discuss the lessons learned from these experiences.

Beagle-2 was the first European Mars lander, part of the ESA satellite mission *Mars Express*, launched in June 2003 [105]. Its mission objective was searching for extinct

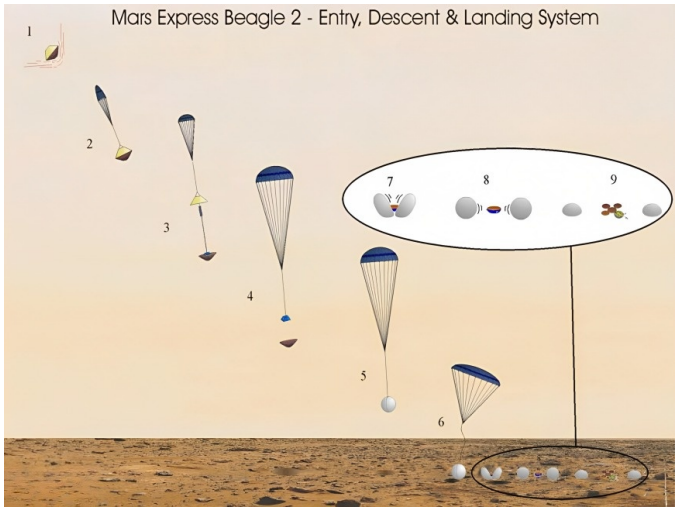

Figure 49. EDL phases of Beagle-2 mission, showing the parachute deployment (steps 2–4) and air bag inflation and touch down (steps 5–9). Image Credit [106].

life by analyzing the martian soil. The entry, descent and landing (EDL) was designed as shown in Figure 49, i.e., during the descent, the system would have expelled the back cover, released the main parachute, and inflated air bags for the touch down. In terms of communications, TM would have been sent only before and after the EDL.

Beagle-2 was successfully ejected by Mars Express on 19 December 2003, and it entered the Martian atmosphere six days later. The first radio contact of Beagle-2 was supposed to happen 8 minutes after landing, with the NASA's *Mars Odyssey* spacecraft pass, but no signal was received. Several attempts were made for establishing the contact, but with no success. Additionally, based on the information available at the time, the Beagle-2 landing site area was estimated $\sim$15000 km^2, making it clearly impossible to locate the probe. As a consequence, four months later, the probe was officially declared lost. An ESA investigation followed in 2004 to determine the cause of the probe's loss. It identified several potential reasons such as the tangling of the parachute or failure of the airbags. However, the investigation also reported that no single technical failure or shortcoming was unambiguously identified. Later on, thanks to the Mars Express telemetry data, it was possible to estimate the landing area as $\sim$340 km^2. Capturing of high-resolution pictures with the *Mars Reconnaissance Orbiter* finally led, in 2015, to the identification of the lander [107] on the Martian surface. The images analysis[10], together with the pre-ejection TM, allowed to hypothesize that the atmospheric entry and descent occurred as planned. On the other hand, due to the lack of TM data during the EDL, it was not possible to confirm what caused the failure.

As a result of the investigation, several recommendations were reported as lessons learned for Beagle-2, including the following relevant to the TT&C

[10]For the possible reader's interest, part of the TM data adopted for the Beagle-2 identification, is available at http://dx.doi.org/10.5061/dryad.707kc [107].

"Future planetary entry missions should include a minimum telemetry of critical performance measurements and spacecraft health status during mission critical phases such as entry and descent".

In light of this, today's space missions always foresee transmitting TM during the EDL. For instance, the more recent lander *Schiapparelli*, which crashed on Mars' surface in 2016, was able to transmit real-time on-board telemetry during its EDL. The the data collected was extremely valuable for its post-flight mission analysis, as it allowed the reconstruction of the trajectory and identification of when the anomaly occurred [108]. Additionally, ESA and NASA future missions are considering the adoption of multiple frequency shift keying (MFSK) modulations for transmitting in X-Band direct-to-Earth, since resilient to the harsh Doppler shifts that take place during the EDL phase [109].

A complete different story was the one of Cassini-Hyugens. In 1997, Cassini-Huygens was launched on a space exploration mission to study Saturn and its icy moons. During its journey, the European probe Huygens, the first human-made object to land on a planet in the far outer solar system, successfully landed on Titan, Saturn's largest moon. The scientific data collected by the probe would have been relayed to Earth by the Cassini orbiter, equipped with an antenna able to stand the challenging transmission. However, in 2000, a few years earlier than Huygens descending into Titan atmosphere, an in-orbit test revealed an anomaly in the Cassini relay-link receiver. The test was designed to emulate Huygens telemetry transmission during the descending stage. The signal, transmitted from the NASA 34-meter dish antenna in Goldstone (California, USA), mimicked both the Doppler dynamics due to the relative geometry and the power strength variations caused by the swinging of the probe while descending on Titan atmosphere [110]. During the in-orbit test, it was discovered that the Cassini receiver had difficulties in decoding the telemetry data due to the high Doppler dynamics involved. In fact, due to limited testing, the impact of frequency uncertainties on the symbol rate was not analyzed, thus preventing the fault detection. When this issue was detected, a team of experts from NASA and ESA was assembled to solve this problem. The team managed to rescue the mission by overhauling Cassini's original trajectory. This modification allowed for almost complete data retrieval from Huygens while causing minimal disruption to Cassini's operations [111]. The new configuration significantly lowered the Doppler dynamics and consequently restored proper operation of the relay-link receiver. A few years after the successful descent of the Huygens probe onto Titan, a detailed analysis of this anomaly was carried out in [112]. The authors concluded that the relay-link receiver was incompatible with the telemetry symbol rate and the original geometry baseline, resulting in compromised performance. The root of the issues was found to be the symbol synchronizer, a first-order DTTL, which relied on automatic gain control (AGC) loops. The gain of the coherent AGC was adjusted in response to power fluctuations, resulting in the "sawtooth" pattern of the DTTL tracking range in Figure 50. The figure shows two points of discontinuity that correspond to the upper and lower switching points of the

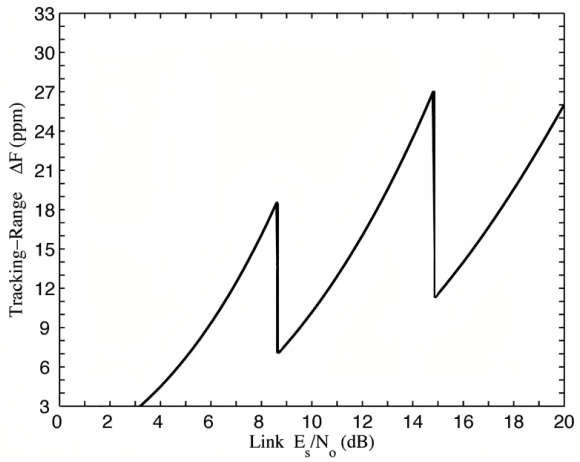

Figure 50. DTTL tracking range. The lower area delimited by the solid curve provides the combination of frequency offset (ΔF) and SNR (E_s/N_0) that the DTTL was able to track. Image Credit [112].

AGC. As the probe approached Titan, power fluctuations and Doppler dynamics increased, causing the DTTL to perform intermittently and thus hindering the receiver's ability to accurately track the timing of the received signal. Only by redesigning the relative geometry of the probe's descent it was possible to obtain a combination of frequency offset (ΔF in Figure 50) and E_s/N_0 that moved the operational points of the DTTL inside the sawtooth region, thereby minimizing the risk of intermittent performance.

The Cassini-Huygens mission provides a valuable lesson for the future. The fault in the Cassini relay-link receiver, only discovered while the mission was in operation, can be partly attributed to limitations in pre-flight testing and simulation. By conducting more extensive testing, the receiver architecture issues could have been identified and resolved before launch. This highlights the importance of thorough testing and validation of spacecraft systems prior to deployment on missions. Furthermore, if the timing algorithm had been reconfigurable in-flight, a single loop parameter adjustment may have resolved the anomaly. Additionally, the significance of a mock-up receiver cannot be overstated, as it played a crucial role in the mission's successful recovery.

VIII. Conclusions

This paper presented an in-depth tutorial on the TT&C for spacecraft, providing first an overview of the space system, and then describing the spacecraft TT&C subsystem, its physical layer, and its main units. These basics have been complemented with a description of the most recent techniques and technologies in the field, highlighting the open issues, and ongoing research. Finally, the paper provided an overview of the standardization organization, and concluded by describing two cases of TT&C issues and failures, with their lesson learned.

This paper should help the engineering community get familiar with the world of the TT&C, often considered a specialized professional field for a few people.

References

[1] P. Foterscue, G. Swinerd, and J. Stark, *Spacecraft systems engineering*. John Wiley & Sons, 4th ed., 2011.

[2] NASA, "NASA Systems Engineering Handbook." Available at www.nasa.gov/connect/ebooks/nasa-systems-engineering-handbook, 2020.

[3] ITU, "Radio Regulations," June 2016. Available at handle.itu.int/11.1002/pub/80da2b36-en.

[4] Copernicus Earth Observation Programme, "Sentinels." Website: www.esa.int/Applications/Observing_the_Earth.

[5] European Space Agency and Chinese Accademy of Science, "Solar wind magnetosphere ionosphere link explorer (SMILE)." Website: sci.esa.int/web/smile.

[6] European Space Agency, "Cosmos: The portal for users of esa's science directorate's missions." Website: www.cosmos.esa.int.

[7] ESA EO Portal, "Solar Orbiter Mission." Website: https://directory.eoportal.org/web/eoportal/satellite-missions/s/solar-orbiter-mission.

[8] European Space Agency, "In-orbit servicing active debris removal." Website: www.esa.int/Safety_Security/Clean_Space/in-orbit_servicing_active_debris_removal.

[9] G. F. Dubos, J. H. Saleh, and R. Braun, "Technology readiness level, schedule risk, and slippage in spacecraft design," *Journal of Spacecraft and rockets*, vol. 45, pp. 836–842, July 2008.

[10] ECSS-E-HB-11A, Space Engineering - Technology Readiness level (TRL) guidelines, March 2017. Available at www.ecss.nl.

[11] ECSS-E-ST-50-05C, Space Engineering - Radio frequency and modulation, October 2011. Available at www.ecss.nl.

[12] J. P. Laboratory, *Deep Space Network Services Catalog*. 2015. Available at deepspace.jpl.nasa.gov.

[13] ESOC, *ESTRACK Facilities Manual*. 2017. Available on request at http://estracknow.esa.int.

[14] M. Maniewicz, "Outcome of the world radiocommunication conference, 2015," in *Proc. Dynamic Spectrul Allocation (DSA) Global Summit*, (Bogota, Columbia), Apr. 2015.

[15] SFCG, "Resolutions and Recommendations," 2022. Available at www.sfcgonline.org.

[16] R. P. Ocampo, "Limitations of spacecraft redundancy: A case study analysis," (Chicago, IL), International Conference on Environmental Systems (ICES), July 2014.

[17] F. Tonicello, B. Mauret, H. Jensen, L. Croci, N. Deplus, N. Neugnot, P. Rumler, and T. Kocma, "ECSS-E-ST&HB-20-20C – A power interface standard & handbook for products development," in *Proc. E3S Web of Conferences*, 2017.

[18] A. Papoulis, *Probability, Random Variables and Stochastic Processes*. New York, NY: McGraw-Hill, 1991.

[19] ECSS-E-ST-70C, Ground systems and operations, July 2008. Available at www.ecss.nl.

[20] I. Shurmer, A. O'Connell, J. Morales, J. Pieiro, and P. P. Emanuelli, "The Sentinel-1A LEOP: Paving the way for the sentinels LEOP preparation and execution," in *Space Operations Organization Conference (SpaceOps)*, May 2016.

[21] B. Nejad, *Introduction to satellite ground segment systems engineering*. Springer-Verlag, 1st ed., 2023.

[22] H. W. Ott, *Electromagnetic compatibility engineering*. John Wiley & Sons, 1st ed., 2009.

[23] ECSS-E-HB-20-07A, Electromagnetic compatibility handbook, September 2012. Available at www.ecss.nl.

[24] B. Dunn, "The resistance of space-quality solder joints to thermal fatigue: Part 1," *Circuit World*, vol. 5, pp. 11–17, Mar. 1979.

[25] Copernicus Earth Observation Programme, "Sentinel-1 - The SAR Imaging Constellation for Land and Ocean Services." Website: http://eoportal.org/web/eoportal/satellite-missions/c-missions/copernicus-sentinel-1.

[26] G. Minatti, S. Maci, P. De Vita, A. Freni, and M. Sabbadini, "A circularly-polarized isoflux antenna based on anisotropic metasurface," *IEEE Trans. Antennas and Prop.*, vol. 60, no. 11, pp. 4998–5009, 2012.

[27] I. Shurmer, F. Marchese, and J. Morales, "Sentinels optical communications payload (OCP) operations: From test to in-flight experience," in *Space Operations Organization Conference (SpaceOps)*, (Marseille, France), May 2018.

[28] G. D. Racca, R. Laureijs, L. Stagnaro, J.-C. Salvignol, J. L. Alvarez, G. S. Criado, L. G. Venancio, A. Short, P. Strada, T. Bönke, *et al.*, "The Euclid mission design," in *Space Telescopes and Instrumentation 2016: Optical, Infrared, and Millimeter Wave*, vol. 9904, p. 99040O, International Society for Optics and Photonics, 2016.

[29] M. K. Simon and S. Million, "Residual versus suppressed-carrier coherent communications," *NASA TDA Progress Report*, vol. 42, p. 127, 1996.

[30] R. De Gaudenzi, A. Guillén i Fabregas, and A. Martinez, "Performance analysis of turbo-coded APSK modulations over nonlinear satellite channels," *IEEE Trans. Wireless Commun.*, vol. 5, pp. 2396–2407, Sept. 2006.

[31] K. Murota and K. Hirade, "GMSK modulation for digital mobile radio telephony," *IEEE Trans. Commun.*, vol. 29, pp. 1044–1050, July 1981.

[32] CCSDS 401.0-B-30, Radio frequency and modulation systems, Part 1, Feb. 2020. Available at http://public.ccsds.org/.

[33] CCSDS 413.0-G-3, Bandwidth-Efficient Modulations - Summary of definition, implementation, and performance, Feb. 2018. Available at http://public.ccsds.org/.

[34] M. Abramowitz and I. A. Stegun, eds., *Handbook of Mathematical Functions*. Dover, 1972.

[35] ECSS-E-AS-50-24C, Adoption Notice of CCSDS 231.0-B-3, TC Synchronization and Channel Coding, March 2021. Available at www.ecss.nl.

[36] R. C. Bose and D. K. Ray-Chaudhuri, "On a class of error correcting binary group codes," *Information and control*, vol. 3, no. 1, pp. 68–79, 1960.

[37] R. G. Gallager, "Low density parity check codes," *IEEE Trans. Inform. Theory*, vol. 8, pp. 21–28, Jan. 1962.

[38] CCSDS 231.0-B-4, TC synchronization and channel coding, July 2021. Available at https://public.ccsds.org/.

[39] ECSS-E-AS-50-25C, Adoption Notice of CCSDS 232.0-B-3, TC Space Data Link Protocol, March 2021. Available at www.ecss.nl.

[40] CCSDS 230.1-G-3, TC Synchronization and Channel Coding - Summary of Concept and Rationale, Oct. 2021. Available at http://public.ccsds.org/.

[41] ECSS-E-ST-50C, Space Engineering - Communications, July 2008. Available at www.ecss.nl.

[42] CCSDS 232.0-B-3, TC space data link protocol, Sept. 2015. Available at https://public.ccsds.org/.

[43] ECSS-E-AS-50-21C, Adoption Notice of CCSDS 131.0-B-3, TM Synchronization and Channel Coding, March 2021. Available at www.ecss.nl.

[44] CCSDS 131.0-B-4, TM synchronization and channel coding, Apr. 2022. Available at http://public.ccsds.org/.

[45] ECSS-E-AS-50-22C, Adoption Notice of CCSDS 132.0-B-2, TM Space Data Link Protocol, March 2021. Available at www.ecss.nl.

[46] ECSS-E-ST-50-02C, *Ranging and Doppler Tracking*, July 2008. Available at www.ecss.nl.

[47] CCSDS 414.1-B-2, Pseudo-Noise PN Ranging Systems, Feb. 2012. Available at http://public.ccsds.org/.

[48] CCSDS 414.0-G-2, Pseudo-Noise PN Ranging Systems, Feb. 2014. Available at http://public.ccsds.org/.

[49] CCSDS 413.1-G-2, Simultaneous transmission of GMSK telemetry and PN Ranging, Nov. 2017. Available at https://public.ccsds.org/.

[50] H. Friis, "A note on a simple transmission formula," *Proceedings of the IRE*, vol. 34, no. 5, pp. 254–256, 1946.

[51] Centre national d'études spatiales, "PROPA: Dynamic link library PROPAGATION." Available at https://logiciels.cnes.fr/en/content/propa.

[52] J. H. Yuen, "A practical statistical model for telecommunications performance uncertainty," tech. rep., 1975. Available at descanso.jpl.nasa.gov.

[53] F. M. Gardner, *Phaselock techniques*. John Wiley & Sons, 3rd ed., 2005.

[54] J. Vilà-Valls, M. Navarro, P. Closas, and M. Bertinelli, "Synchronization challenges in deep space communications," *IEEE Aerospace and Electronic Systems Magazine*, vol. 34, no. 1, pp. 16–27, 2019.

[55] Y. Luo, Y. Wang, Y. Ha, Z. Wang, S. Chen, and H. Pan, "Generalized hyperbolic cordic and its logarithmic and exponential computation with arbitrary fixed base," *IEEE Trans. VLSI*, vol. 27, no. 9, pp. 2156–2169, 2019.

[56] European Space Agency, "International workshop on tracking, telemetry, and command for space," (Noordwijk, The Netherlands), Dec. 2022.

[57] Tesat-Spacecom and Kongsberg Spacetec, *FleXLink: Multi-Gigabit Data Downlink End-to-End Chain. White Paper: Maximizing Throughput in Satellite to Ground Transmissions*. Backnang, Germany and Tromsø, Norway, June 2017.

[58] CCSDS 431.1-B-1, Variable Coded Modulation Protocol, Feb. 2021. Available at http://public.ccsds.org/.

[59] CCSDS 131.2-B-2, Flexible advanced coding and modulation scheme for high rate telemetry applications, Apr. 2022. Available at http://public.ccsds.org/.

[60] A. Modenini, A. Ugolini, and G. Colavolpe, "A fast method for optimizing the amplifier output back-off by means of the total degradation," in *International Workshop on Tracking, Telemetry, and Command for Space*, (Darmstadt, Germany), Sept. 2019.

[61] CCSDS 130.11-G-1, SCCC-Summary of definition and performance, Apr. 2019. Available at https://public.ccsds.org/.

[62] R. Carbone, N. Salerno, F. Marcelli, E. Rondoni, R. Cassettari, J. G. Villarino, J. J. Rigau, and A. Modenini, "High rate flexible high-order SCCC communications system for science X-band," in *International Workshop on Tracking, Telemetry, and Command for Space*, (Noordwijk, The Netherlands), Dec. 2022.

[63] M. Cossu, G. Montorsi, M. Bertinelli, M. Visintin, A. Bicchieri, and N. Jeannin, "Adaptive coding modulation for Earth observation satellites in leo orbit," in *Space Operations Organization Conference (SpaceOps)*, (Daejeon, South Korea), May 2016.

[64] M. Visintin, G. Montorsi, M. Cossu, and N. Jeannin, "Algorithms for the implementation of adaptive coding modulation on Earth observation satellites," in *International Workshop on Tracking, Telemetry, and Command for Space*, (Noordwijk, The Netherlands), Nov. 2016.

[65] M. Davidson, N. Gebert, and L. Giulicchi, "ROSE-L – the L-band SAR mission for Copernicus," in *European Conference on Synthetic Aperture Radar (EUSAR)*, (held virtually), Mar. 2021.

[66] CCSDS 720.1-G-3, *CCSDS File Delivery protocol (CFDP) - Part 1: introduction and overview*, Apr. 2007. Available at https://public.ccsds.org/.

[67] R. Roscigno, S. Fenu, E. Tirro, S. D'Amico, F. Spataro, S. Osborne, and A. Modenini, "Payload data handling & transmission system on ROSE-L mission: main features and CFDP protocol application for data downlink," in *Workshop on RF and Microwave Systems, Instruments & Sub-systems and Ka-band Workshop*, (Noordwijk, The Netherlands), Jan. 2022.

[68] S. Pavale, E. Unnikrishnan, and P. Laksminarasimhan, "Design, implementation and performance evaluation of CCSDS CFDP protocol," in *Proc. IEEE Intern. Conf. on Computational Intelligence and Computing Research*, (Coimbatore, India), Jan. 2010.

[69] B. Ripani, A. Modenini, and G. Montorsi, "On the use of PN ranging with high-rate spectrally-efficient modulations in satellite payload telemetry links," *IEEE Trans. on Aerospace and Electronic Systems*, pp. 1–1, May 2022.

[70] G. Welch, G. Bishop, *et al.*, "An introduction to the Kalman filter," 1995.

[71] F. R. Kschischang, B. J. Frey, and H.-A. Loeliger, "Factor graphs and the sum-product algorithm," *IEEE Trans. Inform. Theory*, vol. 47, pp. 498–519, Feb. 2001.

[72] G. Colavolpe, A. Barbieri, and G. Caire, "Algorithms for iterative decoding in the presence of strong phase noise," *IEEE J. Select. Areas Commun.*, vol. 23, pp. 1748–1757, Sept. 2005.

[73] J. Vila-Valls, P. Closas, M. Navarro, and C. Fernandez-Prades, "Are PLLs dead? a tutorial on Kalman filter-based techniques for digital carrier synchronization," *IEEE Aerospace and Electronic Systems Magazine*, vol. 32, no. 7, pp. 28–45, 2017.

[74] G. Colavolpe, "Communications over phase-noise channels: a tutorial review," in *Proc. Intern. Work. on Signal Processing for Space Commun.*, (Baiona, Spain), p. Proc. 6th Advanced Satell. Mobile Syst. Conf. and 12th Intern. Workshop on Signal Proc. for Space Commun. (ASMS&SPSC 2012), September 2012.

[75] L. Lomidze, D. J. Knudsen, J. Burchill, A. Kouznetsov, and S. C. Buchert, "Calibration and validation of Swarm plasma densities and electron temperatures using ground-based radars and satellite radio occultation measurements," *Radio Science*, vol. 53, pp. 15–36, Jan. 2018.

[76] J. S. Border and J. A. Koukos, "Technical characteristics and accuracy capabilities of delta differential one-way ranging (DeltaDOR) as a spacecraft navigation tool," *JPL Technical Report*, 1993. Available at https://trs.jpl.nasa.gov/.

[77] C. P. Volk, "Sample transponder implementations for PN DDOR," *JPL Technical Report*, 2020. Available at https://trs.jpl.nasa.gov/.

[78] J. Rosello, "IoT for Earth observation - motivation & logic," in *IoT4EO 2023 Wokshop*, (Noordwijk, The Netherlands), Feb. 2023.

[79] V. Languille, "Concepts for the use of IOT in Earth," in *IoT4EO 2023 Workshop*, (Noordwijk, The Netherlands), Feb. 2023.

[80] European Space Agency, "IoT4EO 2023 Wokshop," (Noordwijk, The Netherlands), Feb. 2023.

[81] M. Centenaro, C. E. Costa, F. Granelli, C. Sacchi, and L. Vangelista, "A survey on technologies, standards and open challenges in satellite IoT," *IEEE Communications Surveys & Tutorials*, vol. 23, no. 3, pp. 1693–1720, 2021.

[82] SpaceX, "Starlink," 2021. Website: www.spacex.com/starlink.

[83] OneWeb, "OneWeb," 2022. Website: www.oneweb.world/.

[84] P. Xu, C. Wang, J. Yuan, Y. Zhao, R. Ding, and W. Wang, "Uplink interference analysis between LEO and GEO systems in Ka band," in *Proc. IEEE Intern. Conf. on Computer and Communications (ICCC)*, (Shangai, China), Aug. 2018.

[85] SpaceX, "SpaceX non-geostationary satellite system: Attachment A, technical information to supplement schedule S," November 2016. Available at https://fcc.report.

[86] Federal Communications Commission, "Public Notice: Promoting Telehealth in Rural America." FCC Record, March 21 2022. Available at https://apps.fcc.gov.

[87] L. Jia, Y. Zhang, J. Yu, and X. Wang, "Design of mega-constellations for global uniform coverage with inter-satellite links," *Aerospace*, vol. 9, no. 5, 2022.

[88] G. M. Capez, M. Caceres, C. Bridges, S. Frey, R. Armellin, R. Garello, and P. Bargellini, "On the use of mega constellation services in space," 2022.

[89] K. Andrews, J. Hamkins, S. Shambayati, and V. Vilnrotter, "Telemetry-based ranging," in *Proc. IEEE Aerospace Conf.*, Mar. 2010.

[90] V. Vilnrotter, J. Hamkins, and S. Ashrafi, "Performance analysis of digital tracking loops for telemetry-based ranging applications," in *Proc. IEEE Aerospace Conf.*, Mar. 2014.

[91] J. Hennawy, N. Adams, E. Sanchez, D. Srinivasan, J. Hamkins, V. Vilnrotter, H. Xie, and P. Kinman, "Telemetry ranging using software-defined radios," in *Proc. IEEE Aerospace Conf.*, Mar. 2015.

[92] B. Hespeler, H. Hofmann, A. Camuso, J. Lange, and A. Modenini, "Integrated X-Band payload data transmitter & TTC transponder (IXPT)," in *International Workshop on Tracking, Telemetry, and Command for Space*, (Noordwijk, The Netherlands), Nov. 2022.

[93] N. Salerno, L. Simone, D. Gelfusa, M. Belardinelli, M. Salvati, and R. Viola, "TT&C transponder with integrated payload data transmitter for Earth Observation missions," in *International Workshop on Tracking, Telemetry, and Command for Space*, (Noordwijk, The Netherlands), Nov. 2022.

[94] A. Aroumont, P. Maguire, B. Hespeler, E. Couty, and S. Carrasco Martos, "Very high data rate receiver for K-band uplink for future Moon exploration missions," in *International Workshop on Tracking, Telemetry, and Command for Space*, (Noordwijk, The Netherlands), Nov. 2022.

[95] F. Pelorossi, F. Concaro, I. Montesinos, M. Pasian, and C. Chambon, "Implementation of the K-band uplink channel for Moon missions in the existing ESA deep space antennas," in *International Workshop on Tracking, Telemetry, and Command for Space*, (Noordwijk, The Netherlands), Nov. 2022.

[96] S. Marti and E. Vassallo, "Future multiple uplink per aperture access schemes," in *Space Operations Organization Conference (SpaceOps)*, (Stockholm, Sweden), June 2012.

[97] D. Gelfusa, F. Cialfi, N. Salerno, and L. Simone, "Integrated deep space & radio-science TT&C transponder (IDST)," in *International Workshop on Tracking, Telemetry, and Command for Space*, (Darmstadt, Germany), Sept. 2019.

[98] C. Campa, D. Gianfelici, and R. Abello, "Multiple spacecraft per aperture with code division multiple access modulation," in *International Workshop on Tracking, Telemetry, and Command for Space*, (Noordwijk, The Netherlands), Dec. 2022.

[99] CCSDS 130.1-G-3, TM Synchronization and Channel Coding - Summary of Concept and Rationale, June 2020. Available at http://public.ccsds.org/.

[100] CCSDS 131.3-B-2, CCSDS Space Link Protocols over ETSI DVB-S2 Standard, Apr. 2022. Available at http://public.ccsds.org/.

[101] CCSDS 130.12-G-1, CCSDS Protocols over DVB-S2 - Summary of Definition, Implementation, and Performance, Nov. 2016. Available at https://public.ccsds.org/.

[102] CCSDS 131.21-O-1, Serially Concatenated Convolutional Codes - Extension (SCCC-X), May 2021. Available at https://public.ccsds.org/.

[103] CCSDS 131.31-O-1, CCSDS Space Link Protocols over ETSI DVB-S2X Standard, Sept. 2021. Available at https://public.ccsds.org/.

[104] A. Witze, "Global 5G wireless deal threatens weather forecasts," *Nature*, vol. 575, pp. 577–578, Nov. 2019.

[105] M. Sims, C. Pillinger, I. Wright, J. Dowson, S. Whitehead, A. Wells, J. Spragg, G. Fraser, L. Richter, H. Hamacher, *et al.*, "Beagle 2: a proposed exobiology lander for ESA's 2003 Mars Express mission," *Advances in Space Research*, vol. 23, no. 11, pp. 1925–1928, 1999.

[106] P. A. Liever and S. D. Habchi, "CFD prediction of the Beagle 2 Mars probe aerodynamic database," in *Thermal and Fluids Analysis Workshop*, (Huntsville, AL), Sept. 2001.

[107] J. Bridges, J. Clemmet, M. Croon, M. Sims, D. Pullan, J.-P. Muller, Y. Tao, S. Xiong, A. Putri, T. Parker, *et al.*, "Identification of the Beagle 2 lander on Mars," *Royal Society Open Science*, vol. 4, no. 10, p. 170785, 2017.

[108] D. Bonetti, G. De Zaiacomo, G. Blanco, I. P. Fuentes, S. Portigliotti, O. Bayle, and L. Lorenzoni, "ExoMars 2016: Schiaparelli coasting, entry and descent post flight mission analysis," *Acta Astronautica*, vol. 149, pp. 93–105, Aug. 2018.

[109] L. Mauger, M. Soriano, S. Rogstad, S. Finley, J. Tarsala, C. Sackier, P. Ilott, D. Buccino, and K. Oudrhiri, "Direct to earth communications using MFSK tones during M2020 entry, descent, and landing," in *Proc. IEEE Aerospace Conf.*, (Big Sky, MT), Mar. 2022.

[110] J. Oberg, "Titan calling," *IEEE Spectrum*, vol. 41, no. 10, pp. 28–33, 2004.

[111] L. J. Deutsch, "Resolving the Cassini/Huygens relay radio anomaly," in *Proc. IEEE Aerospace Conf.*, (Big Sky, MT), Mar. 2002.

[112] L. Popken, "Rescuing the Huygens mission from fiasco," *Proceedings of the IEEE*, vol. 95, no. 11, pp. 2248–2258, 2007.

Andrea Modenini received his Ph.D. in January 2014 from the University of Parma.

Since March 2015, he is at the European Space Agency (ESA), currently working as TT&C Communications Systems Engineer, supporting ESA Earth Observation and Scientific satellite missions, research and development of TT&C units, techniques, including those for unmanned aerial vehicles (UAVs). He is also contributing to the education in the field of TT&C as tutor of ESA trainees. Finally, he is involved in several standardization activities for satellite TT&C in the framework of ECSS, SFCG, and CCSDS. For the latter, he is Chair of the Coding & Synchronization working group.

Barbara Ripani received her Master's Degree from Politecnico di Torino in Communications and Computer Networks Engineering in 2021. She is working toward the Ph.D., started in September 2021 at Politecnico di Torino, under the supervision of Prof. Guido Montorsi and Ph.D. Andrea Modenini. Currently, she is working as a contractor in ESTEC. Her research topic focuses on synchronization challenges in Deep Space communication links. In January 2022, she became a student member of IEEE, AESS, and ComSoc societies.